



HAL
open science

Cliff erosion: self-organisation of sand cliff material eroded by monochromatic waves

Bastien Caplain, Vincent Regard, Dominique Astruc

► **To cite this version:**

Bastien Caplain, Vincent Regard, Dominique Astruc. Cliff erosion: self-organisation of sand cliff material eroded by monochromatic waves. 2013. hal-00790628

HAL Id: hal-00790628

<https://hal.science/hal-00790628>

Preprint submitted on 20 Feb 2013

HAL is a multi-disciplinary open access archive for the deposit and dissemination of scientific research documents, whether they are published or not. The documents may come from teaching and research institutions in France or abroad, or from public or private research centers.

L'archive ouverte pluridisciplinaire **HAL**, est destinée au dépôt et à la diffusion de documents scientifiques de niveau recherche, publiés ou non, émanant des établissements d'enseignement et de recherche français ou étrangers, des laboratoires publics ou privés.

Cliff erosion: self-organisation of sand cliff material eroded by monochromatic waves

B. Caplain,¹ V. Regard,² D. Astruc¹

Abstract. Laboratory experiments on cliff erosion were carried out in a monochromatic wave flume. Natural coarse sands are used to represent cliff erosion and bottom morphodynamics with a reasonable time scale. A bottom typology is established as a function of wave forcing, through the wave energy flux F and the surf similarity parameter ξ . The bottom types strongly depends on the surf similarity parameter at the breaker point ξ_b . Steep terraces ($\xi_b > 0.48$), one-bar profiles ($0.42 < \xi_b < 0.48$), gentle terraces ($0.38 < \xi_b < 0.43$) and double-bars profiles ($\xi_b < 0.38$) were observed. It can be translated into a Dean parameter Ω vs. Shields number Θ_b space to take into account sediment granulometry. Sediment grain diameter change has no noticeable influence on bottom typology. The bottom types depends more on the Dean parameter Ω than on the Shields number Θ_b . Finally, we explored cliff height effect: it does not modify the bottom typology established.

1. Introduction

Predicting the coastline evolution depends on the geological nature of the coastline. Natural coastal areas may be composed of sand, silt, mangroves or rocks, as cliffs. Rocky shores occupy about 80% of the coastline of the Earth [Emery and Kuhn, 1980]. This contribution aims at bringing new informations on how such kind of coasts behave.

Rocky shores, also known as cliffed coasts are usually composed of a platform ('wave cut platform') backed by a cliff [e.g., Sunamura, 1992]. Cliff erosion is mainly controlled by wave impact but depends likewise on numerous factors [Sunamura, 1992], such as weathering by wetting and drying cycles during tidal cycles [Kanyaya and Trenhaile, 2005], rainfall [Duperret et al., 2002; Costa et al., 2004; Young et al., 2009], bioerosion [e.g., Nesteroff and Mélières, 1967; Andrews and Williams, 2000], material stratification or fractures [Duperret et al., 2004]. Moreover, the characteristic scales of cliff erosion are very large, encompassing the single wave scale or a kilometers-long retreat on geological times (thousands to millions of years). Here we take the advantage of using a physical model to simplify the analysis of rocky shore retreat, in order to analyze accurately each mechanism.

If the wave height and the cliff height are the same order, waves can reach and erode the cliff top ([Hansom et al., 2008]). We limited our study to the influence of wave forcing on the cliff erosion by undermining, i.e., when the wave height is less than the cliff height. Cliff erosion by undermining is the result of a series of cycles, each one corresponding to 3 successive phases:

- Phase 1: cliff toe erosion

The mechanical action of impacting waves cut the cliff toe creating a notch, as the forces resulting from the impact can

be greater than the material strength [Brossard and Duperret, 2004; Erikson et al., 2007]. The impact is considered more efficient when entrained solid particles (pebbles, ...) are present ('tool effect') ([Sunamura, 1992; Larson et al., 2010]).

- Phase 2: cliff fracturation and collapse

When the weight of the overhanging cliff is close to the material resistance of the rock, cliff deformations occur and fractures can appear ([Kogure et al., 2006; Young and Ashford, 2008]). The cliff destabilization leads to a collapse event. The main collapse types are reorganised by tensile stress at the cliff top leading to a rockfall, or by shear stress leading to a landslide [Hampton, 2002; Young and Ashford, 2008; Wolters and Muller, 2008].

- Phase 3: debris evacuation

Following cliff collapse, a heap of fallen debris is lying in front of the cliff base. These debris have a shielding effect, protecting the cliff from wave assaults [Walkden and Dickson, 2008]. They are progressively evacuated along and across the shore by waves and currents. This sediment transport modifies the bottom morphology [de Lange and Moon, 2005; Pierre, 2006]. In turn, waves and currents are transformed by the bottom morphology. When the waves start again to impact on the cliff, the cycle of cliff erosion starts again [Walkden and Dickson, 2008].

Laboratory wave flume experiments have been conducted to study cliff erosion by waves by modeling the cliff with a mixture of plaster, sand and water [Sanders, 1968] or a mixture of cement, sand and water [Sunamura, 1992]. In fact, these former experiments were dedicated to notch evolution analysis (phase 1). The high resistance of the mixtures used results in a slow evolution of a single notch often observed over a period of several days. Sunamura [1992] performed experiments in a wave basin allowing oblique waves. He observed a cliff recession due to removing debris by longshore currents, but this recession is carried out on very long time.

Damgaard and Dong [2004] used mixtures of sand, clay and water to model the cliff. The cliff was placed on a horizontal solid plane with a constant slope. The setup allowed variations in cliff height, wave height, period and incidence. They observed a cliff recession within a reasonable time of the order of hours. Cliff recession rate decreases exponentially with time for waves at normal incidence and seems constant for oblique waves. This behavior is related to the presence of a longshore current which removes the fallen debris (phase 3). In addition, the wave forcing and the cliff

¹INPT, UPS, IMFT, Université de Toulouse, allée Camille Soula, 31400 Toulouse, France. CNRS, IMFT, 31400 Toulouse, France.

²UPS (OMP), GET, Université de Toulouse, 14, avenue Edouard Belin, 31400 Toulouse, France. CNRS, GET, 31400 Toulouse, France. IRD, GET, 31400 Toulouse, France.

height are varied and they conclude that the recession rate increases with wave height and period and decreases with the cliff height. However, the mechanisms of cliff erosion and bottom morphodynamics were not analyzed in detail whereas *Caplain et al.* [2011] highlight that sandy cliff recession strongly depends on the bottom morphology. In the following, we expand the experiments of *Caplain et al.* [2011] using the same experimental set-up which is presented hereafter.

In their experiments, *Caplain et al.* [2011] have shown that the cliff, the bottom morphology (bathymetry) and the waves are highly coupled and they constitute two systems, evolving with different characteristic times. On the one hand, the cliff recession is controlled by bottom erosion at the scale of the bottom morphology evolution. On the other hand, the bottom evolution is linked with sediment transport at the wave scale. The aim of this study is to understand how these two system interact. In particular we want to show how hydrodynamics influence shore morphodynamics that in turn change the wave behavior at cliff base. In addition, we show that the amount of eroded cliff could be a limiting factor in morphological features like ridges.

Bottom morphodynamics is controlled by hydrodynamic forcing (waves, tide) and sediment properties [e.g., *Le Roux*, 2010]. When waves interact with the bottom, their energy dissipates in three ways, by viscous dissipation and sediment transport at the bottom, and by cliff bottom erosion [e.g., *Stephenson and Kirk*, 2000; *Trenhaile*, 2000]. In beaches, the retroaction between energy dissipation and morphology leads to an equilibrium; the morphology then can be described by the Dean number Ω :

$$\Omega = \frac{H_b}{Tw_s} \quad (1)$$

with H_b the breaker height and w_s the sediment fall velocity in water.

The Dean number is the ratio of a fall time of a particule H_b/w_s and the wave period T . A classification of different cross-shore profiles, from field observations, was established by [*Wright and Short*, 1984] based on Ω for microtidal regimes. For $\Omega \leq 1$, the reflection is important, the surf zone is small and breaking waves are surging; the profile is qualified of 'reflective' and characterized by a steep slope. For $\Omega \geq 5$, profiles with a gentle slope are observed with a large surf zone and breaking waves are spilling: these are dissipative profiles. The intermediate zone $1 \leq \Omega \leq 5$ presents different bottom profiles shaped by bars or terraces.

Sandbars are a major feature of bottom morphodynamics. Their formation is caused by sand accumulated by sediment fluxes. It has been observed that for moderate wave conditions, bars migrate landward; inversely they migrate seaward for energetic wave conditions [e.g., *Gallagher et al.*, 1998; *Ruessink et al.*, 2003].

A classification of bottom morphology was also performed for low energy wave regimes [*Hegge et al.*, 1996; *Makaske and Augustinus*, 1998]. [*Hegge et al.*, 1996] distinguished four beach morphotypes (concave, moderately concave, stepped and moderately steep) by profiles shape and sediment grain size, but not as a function of hydrodynamical conditions. [*Makaske and Augustinus*, 1998] have schematized bottom types from beach face in the Rhone-Delta in terms of wave height at breaker point H_b . Observed profiles are steep terraces for $H_b \leq 0.25$ m, concave profiles for 0.25 m $\leq H_b \leq 0.35$ m and convex-concave profiles for $H_b \geq 0.35$ m.

Wave flume experiments were conducted to compare observations of stationary profiles to *Wright and Short* [1984]'s classification [*Grasso et al.*, 2009; *Kamalinezhad*, 2004; *Wang and Kraus*, 2005]. *Grasso et al.* [2009] used a low density sediment in a wave flume with irregular waves. They

have refined the intermediate profiles of *Wright and Short* [1984]'s classification. For $\Omega = 2.5$, terraced profiles were observed, and for $\Omega = 3.7$, the observed profiles are cut into two parts, a gentle slope seaward and a steep beach face. By cons, few laboratory experiments were conducted for regular waves [*Baldock et al.*, 2010].

We aim to realised a typology of bottom morphology as a function of forcing waves for regular waves. Then, we will analyse the influence of grain size of sediment and cliff height on the bottom typology. In this paper, the experimental setup, the metrology and the parameters used in the study are described in section 2. The classification method of bottom morphologies and associated hydrodynamics are developed in section 3. The influence of grain size and available sediment volume (by means of the cliff height) on bottom typology are analysed in section 4. A discussion and conclusions are given in section 5 and 6.

2. Methodology

2.1. Experimental Setup

The experiments were carried out in a 5 m-long, 25 cm-high and 14 cm-wide wave flume equipped with a flap wave paddle generating monochromatic waves (Fig. 1). The offshore water depth is $d = 15$ cm. We set axes whose origin is located at the wave onshore end for x and at water level for z . To observe different nearshore wave dynamics (breaker types), a rigid nearshore slope of $\tan(\beta) = 10\%$ is used. T is the wave period between 0.5 s and 2 s and H is the incident wave height up to 6 cm.

The massif is a mixture of coarse sand and water, capillary forces are used to ensure the cohesive material and thus to maintain the cliff shape. The set up protocol of the sand massif is the same for each experiment: the flume is filled with water then the sand is immersed over the sloping base. A horizontal cut is realized to adjust the cliff height h_C between 5 cm and 15 cm (measured from the free surface to the cliff top), then the flume is slowly emptied to drain the massif. A vertical cut fixes the initial cliff position $x_C = 40$ cm. After about 2 hours draining, the flume is filled up to $d = 15$ cm and the wave generator is activated.

2.2. Metrology

Three capacitive probes (100 Hz sampling) with a spacing of 3 cm (Fig. 1) measure the free surface elevation in the flat bottom portion of the flume. The incident and reflected wave energy fluxes are estimated using the method of *Mansard and Funke* [1980].

A high resolution camera has been positioned a side the flume in order to measure sand and water surfaces positions by a shadowgraph method. This method consists in visualizing a lighted field in order to accentuate surfaces and so better detect them (Fig. 2). As the erosion processes is observed to slow down, the acquisition frequency which is set close to wave frequency for about the first 4 hours, is then reduced to about 1/10 of this value until the end of the experiment. Video images are processed to extract both sand $Z(x, t)$ and water $\eta(x, t)$ surfaces position (Fig. 2). An example of time evolution of the sand profiles is shown in Fig. 3. As the acquisition frequency is too low to lead water surface evolution at the wave scale, we analyze hydrodynamics when the system is stabilized. This envelope of free surface elevation can be calculated from water free surface elevation $\eta(x, t)$ (Fig. 6). These envelope of waves allows to measure the spatial evolution of wave height $H(x)$.

2.3. Parameter range

In order to model the cliff erosion in laboratory, the temporal and spatial scales have been reduced. However,

the involved processes could be representative of natural processes. The system modelled in our study involves a large number of physical parameters. Ensuring a complete similarity for all these parameters is obviously impossible [Grasso *et al.*, 2009]. The chosen ones are those that seem the most relevant to study the interaction between waves and the sandy cliff.

The interactions between waves, cliff and bottom morphology depend on the hydrodynamics and material characteristics. The cliff recession and the sediment transport are linked to the incident wave energy flux F defined by:

$$F = \frac{1}{8} \rho g H^2 C_G \quad (2)$$

with ρ the water density, g the gravity acceleration and C_G the group velocity.

The wave energy dissipation and the bottom shape depend on the type of breaking waves. Breaker types can be determined by the surf similarity ξ (Iribarren) parameter:

$$\xi = \frac{\tan(\beta)}{\sqrt{H/\lambda}} \quad (3)$$

where λ is the wavelength.

The sediment transport by waves can be characterized with the Shields number Θ ([Grasso *et al.*, 2009]):

$$\Theta = \frac{1}{2} f_w \frac{(A_p \omega)^2}{g(\rho_s/\rho - 1) D_{50}} \quad (4)$$

where f_w is a wave friction factor at the bottom ([Grasso *et al.*, 2009]), $\omega = 2\pi/T$ is an angular frequency and $A_p = H/(2 \sinh kd)$ is the particule excursion at the bottom with k the wave number. The Shields number measures the capability of a shear flow fluid to set the sediment in motion. It determines the transport regime (bed load or suspension for, respectively low or high values of Θ).

The sediment characteristics determine the type of sediment transport, the bottom morphology and the cliff cohesion. Unfortunately, it is not possible to represent satisfactorily these three processes. The material choice was made for reproducing both natural bottom profiles and a cliff recession on a time scale of a day. The similitude of hydro-sedimentary parameters (Ω , Θ) is ensured only for a low density and/or a fine-grained sediment ([e.g., Grasso *et al.*, 2009]). A low density sediment implies a too important aspect ratio between the critical notch depth L_n^c and the cliff height h_c to represent a natural cliff collapse. A material with a fine-grained sediment (about $D_{50} \leq 0.1$ mm) is too strong and does not allow to observe several collapses on the reasonable time scale. We therefore chose three types of natural and relatively coarse sands (Table 2). Finally, these materials ensure both the observation of reasonable cliff recession rates and Dean number values ($\Omega < 3$; sediment transport dominated by bed load transport).

3. Spatio-temporal evolution of the system

During an experiment, the cliff erosion process occurs on different time scales: (i) During the first few minutes, the waves tend to break at the cliff leading to a rapid erosion. Several collapse events occur on the time scale of a few waves. Cliff debris are rapidly transported, forming a sandy platform over the rigid slope. (ii) This platform then develops for a few hours with the increasing volume of eroded sediment. In turn, the morphological change causes seaward motion of the breakers, the wave energy dissipation is stronger and waves break on the bottom leaving to appear surf and swash zones. The frequency of cliff collapse events diminishes and the cliff recession rate progressively

decreases. (iii) These collapse events are less frequent with time and the morphological system tends to stabilize. The total sediment volume is spread seaward on a length of more than one meter over the rigid slope. When the volume of sediment is enough to fully dissipate wave energy before reaching cliff bottom, the cliff is no more eroded. Waves fail either at the cliff toe or at a berm created by waves in front of the cliff. The bottom morphology no more evolves and hydrodynamics is stabilized; the system tends to stabilize towards a steady state (Fig. 3). We analyse the bottom morphology when the stationary state is reached. Some experiments reached a unsteady state characterized by a sandbar oscillation for which we propose an explanation in the Discussion section. In these cases, we analyze the bottom morphology as an average of the bottom morphologies corresponding to the two extrema of the sandbar position.

Note that a collapse event is instantaneous: this is a discrete process. So cliff front evolution, depending on these collapse events, is somewhat discontinuous. Our observations have shown that the characteristic time of the cliff recession cycle is very small compared to the one of the bottom evolution.

4. Bottom topography and related hydrodynamics

The bottom morphology is sculpted by waves as a function of the breaking wave type and position of swash and surf zones. The aim of this work is to relate the different observed bottom morphologies to hydrodynamics. For that, we propose a method of bottom characterization. Firstly, we choose to introduce different morphological singularities to establish a classification of the different observed bottom types, then in order to correlate it at the hydrodynamics characteristics. The morphological singularities are related to slope and/or curvature changes of the bottom profile. Hydrodynamics characterization is based on types of breaking waves and hydrodynamical singularities which distinguished the different zones of coastal hydrodynamics. From these accounts, we can deduce different types of bottom morphology, and morphological and hydrodynamical correlations.

4.1. Bottom singularities

We aim at analyzing how the bottom morphology is influenced by wave forcing and in turn, how it modifies the hydrodynamics and consequently the wave forcing. It is therefore necessary to characterize the bottom topography as a function of wave forcing. We propose a bottom typology based on observed bottom profiles. We can observe various bottom morphologies with or without sandbars, gentle or steep terrace, scarp, plateau, berm in front of the cliff. In order to characterize these different bottom morphologies, we choose to use some particular points of the bottom profile $Z(x)$. The determination of these points is based on properties of the first $Z'(x)$ and second $Z''(x)$ derivatives.

From the analysis of the various bottom profiles, we have chosen seven points of morphological singularities on the bottom profile (Fig. 4). These are listed thereafter, in a shoreward direction.

Cliff (C)

The cliff (C) front corresponds to a discontinuity of the sand elevation between cliff bottom and cliff top. Whether the cliff is vertical or not, it corresponds to a local maximum slope (we take $Z'(x)$ absolute value) (Fig. 4). At the beginning of the experiments, $x_C = 40$ cm, for a fully eroded cliff, $x_C = 0$ cm.

Notch (N)

A notch (N) may be present at the cliff bottom. Its location (x_N, z_N) corresponds to the point of the bottom profile with lower elevation than the cliff ($z_N < h_C$) where x is minimum (Fig. 4).

Berm (B)

In some cases, a berm (B) is present. The berm crest is convex and the berm seaward profile is concave. We choose to determine the berm position (x_B, z_B) as the curvature change point, i.e., the inflection point for $Z''(x_B) = 0$ (Fig. 4).

Slope Stabilization (SS)

The absolute value of the slope decreases seaward from the shoreline until a slope stabilization (SS). This point corresponds to the beginning of a constant slope zone in seaward direction. We identify the point of this transition as the point where the second derivative of sand profile $Z''(x)$ is close to 0, we take it for $Z''(x_{SS}) \leq 0.1$. We name this point (x_{SS}, y_{SS}) the point of slope stabilization (Fig. 4).

Slope Change (SC)

The slope of the sand profile is nearly constant until a slope change (SC). This change corresponds either to a scarp (SC₊), or to a plateau (SC₋). We identify the position of this slope change (x_{SC}, z_{SC}) by the second derivative maximum (respectively minimum) of the sand profile $Z''(x_{SC})$ which corresponds to a plateau (respectively a scarp) (Fig. 4).

Zero Slope (ZS)

The slope of the sand profile is low until to reach a zero slope (ZS). We identify the position of the zero slope (x_{ZS}, z_{ZS}) where the first derivative is equal to zero ($Z'(x_{ZS}) = 0$) (Fig. 4).

Platform Step (PS)

The last singular point of the sand profile that we chose is the platform step (PS), its position (x_{PS}, z_{PS}) is defined by an inflexion point ($Z''(x_{PS}) = 0$) (Fig. 4).

From the analysis of observed bottom profiles, only (PS) point is systematically identified. We will show (B) point (or (N) if (B) does not exist, or (C) if (B) and (N) do not exist) corresponds to the shoreline. We define the (S) point as a fictive point corresponding to the shoreline.

4.2. Morphological lengths

To characterize the different types of bottom morphology, we define different characteristic lengths from the determination of the morphological singularities. The platform extends from (PS) to (S), the platform length is defined as $L_P = x_{PS} - x_S$. We subdivide this platform into two parts delimited by (SC): the inner platform extending from (SC) to (S) and the outer one from (PS) to (SC). The inner platform length is $L_{Pi} = x_{SC} - x_S$ and the outer platform length is $L_{Po} = x_{PS} - x_{SC}$. When (SC) does not exist, we replace it by (SS).

Between (S) and (SS), the slope $Z'(x)$ decreases until a stabilization, that is to say the profile has a concave shape. We thus define this portion as the “concave profile”, its length is $L_C = x_{SS} - x_S$.

We will show some bottom profiles are decomposed in two sub-systems. Two morphological points are added on the outer system, zero slope and platform step points named (ZS') and (PS') respectively (Fig. 5). For these cases, the total platform of the two-systems profile extends from (PS') to (S) (noted $L'_P = x_{PS'} - x_S$), the inner platform extends

(PS) to (S) (noted $L'_{Pi} = x_{PS} - x_S$) and the outer one from (PS') to (PS) (noted $L'_{Po} = x_{PS'} - x_{PS}$).

4.3. Hydrodynamical singularities and characteristics lengths

The envelope of waves calculated allows to measure the spatial evolution of wave height $H(x)$. Breaker height H_b and corresponding breaker point x_b can be estimated where $H(x)$ is maximum (Fig. 6). The location (x_{SWb}) of the limit of surf and swash zones (the bottom of the swash zone) is the location where the lower wave envelope is coincident with the sand profile (Fig. 6). The top of the swash zone (x_{SWt}) is located at the point where the upper limit of the wave envelope is coincident with the sand profile, i.e. where the wave height is null (Fig. 6).

From these hydrodynamical singularities, we can define the characteristic lengths of surf and swash zones. The surf zone extends from breaker point to the limit of surf and swash zones, its length is defined as $L_{SF} = x_b - x_{SWb}$. The swash zone extends from the limit of surf and swash zones to the top of swash zone, its length is $L_{SW} = x_{SWt} - x_{SWb}$.

4.4. Bottom typology

We seek now to establish a classification of bottom morphologies and to relate it to wave forcing. This characterization is based on the outer platform shape and type of breaking waves when the bottom profile is stabilized. Experiments have been carried out with the C41-sand and we identified four main types of bottom profiles in the (F, ξ) plan (Fig. 7).

Type 1

Some bottom profiles have been observed with an outer platform presenting a steep terrace profile (about 15-20% slope, Fig. 8). These profiles have an inner platform longer than the outer platform. The shoreline (S) is always characterized by a berm (B) and (SC) corresponds to a decreasing slope (SC₋), i.e., a plateau. The sequence of morphological singularities is {(B)-(SC₋)-(PS)}. At the platform outer edge, the breaking waves are surging; they turn immediately into a hydraulic bore over the platform leading to the runup reaching (B). The surf zone is very short (about 10% of the wavelength). The platform length L_P is small compared to the wavelength λ ($L_P/\lambda \approx 0.3$). These profiles are observed for $\xi > 0.65$ (Fig. 7).

Type 2

These profiles present an outer platform characterized by a bar attached to the inner platform (Fig. 9). The shoreline (S) is always characterized by a berm (B) and (SC) corresponds to a scarp (SC₊). The sequence of morphological singularities is {(B)-(SC₊)-(PS)}. Breaking waves are collapsing and tend to dig the bottom and hence create a bar. This breaker type causes a splash-up which immediately merges with the hydraulic bore leading to the runup. The ratio between the platform length L_P and the wavelength λ is the order of $L_P/\lambda \approx 0.40 - 0.45$. These profiles are observed for $0.55 < \xi < 0.6$ (Fig. 7).

Type 3

These profiles show an outer platform as a gentle terrace (Fig. 10 and Fig. 11). The platform length L_P is slightly greater than half the wavelength as $L_P/\lambda \approx 0.55 - 0.60$. These profiles are observed for $0.55 < \xi < 0.6$ and $F < 1.3 W/m$ (Fig. 7).

For this bottom type, we distinguish two types of inner platform, one with a small gentle terrace corresponding to “concave” profile for $F < 1 W/m$ (Fig. 10) and one with a large steep terrace for $F > 1 W/m$ (Fig. 11). Thus, we subdivide the bottom type 3 in 3a for the first case and 3b

for the second (Fig. 7). We can observe the breaking waves are plunging/spilling for bottom type 3a (Fig. 10a) and spilling for bottom type 3b (Fig. 11a), that explains there is no bar. The sequences of morphological singularities of bottom types 3a and 3b are {(S)-(SS)-(ZS)-(PS)} and {(S)-(SC)-(ZS)-(PS)} respectively. We can observe in Figure 10 that in this example of type 3a the lower wave envelope coincides with the bottom for $x \approx 26$ cm, which characterizes the beginning of the swash zone. The upper envelope is close to (N) for $x \approx 23$ cm, hence the swash zone is small compared to that of type 3b (it extends in figure 11 from $x \approx 29$ cm to $x \approx 14$ cm).

Type 4

The bottom type 4 present two separate systems, hence the outer and inner platforms are defined from (PS') to (PS) and from (PS) to (S) respectively. Besides, the waves are breaking twice: two breaker can be distinguished, one at the outer platform ($x \approx 87$ cm) and one at the inner platform ($x \approx 37$ cm). The outer platform is formed of two sandbars ($x \approx 81$ cm and $x \approx 59$ cm), the main one being the farthest seaward (Fig. 12). The inner platform presents a variable shape, it can be described as the types 1, 2, 3a or 3b already defined. Outer breaking waves are plunging at the outer sandbar and generate a splash-up at the secondary sandbar. A wave front then propagates until a second breaker at the inner platform. The relationships between inner platform morphology and inner breaker type is identical to that previously described for types 1 to 3. We consequently propose to subdivide the bottom type 4 into types 41 (shown in Fig. 12), 42, 43a and 43b according to the inner platform morphology. Therefore, the sequence of morphological singularities is composed of two sequences, the inner one and the outer other, it is {(sequence of the inner bottom type 1, 2 or 3)-(ZS')-(PS')}. For instance, the sequence of bottom type 41 is {(B)-(SC)-(PS)-(ZS')-(PS')} (Fig. 12). The platform length L_P is as $L_P/\lambda \geq 0.7$ but the length of the most of the platforms is greater than the wavelength (λ). These types of profiles are observed for ($\xi < 0.5$) and $(F, \xi) = (2.1, 0.53)$ (Fig. 7).

Figure 7 shows the types of bottom morphology depend more strongly on the surf similarity parameter ξ than on the wave energy flux F . To characterize natural systems, bottom morphologies are often characterized as a function of wave parameters at the breaker point (e.g. [Wright and Short, 1984; Makaske and Augustinus, 1998]). We thus establish a classification of bottom morphologies where we replace the incident wave height H by the breaker height H_b . In Figure 13, the bottom typology is represented in the (F_b, ξ_b) diagram with F_b the wave energy flux at the breaker point and ξ_b the surf similarity parameter at the breaker point. We can observe that the bottom type strongly depends on the surf similarity parameter at the breaker point ξ_b . Type 1 profiles are observed for $\xi_b > 0.48$, type 2 profiles for $0.42 < \xi_b < 0.48$, those of type 3 for $0.38 < \xi_b < 0.43$ and those of type 4 for $\xi_b < 0.38$ (cf. Table 1). Profile types 41, 42 and 43 appear to be also dependent on the surf similarity parameter at the breaker point ξ_b . Thus, the profiles 41 are observed for $0.34 < \xi_b < 0.38$, those 42 for $0.3 < \xi_b < 0.34$ and those 43 for $\xi_b < 0.31$ (cf. Table 1). It is then possible to check whether the relationships between wave characteristics and platform morphology are the same for the both inner and outer systems of type 4 profiles. Small symbols shown in Figure 14 correspond to the inner wave parameters at the breaker point of the profile types 41, 42 and 43. We can observe that the types of inner profiles are in line with the characterization made for single system types. We can conclude the bottom morphology only depends on ξ_b , whatever the wave energy flux F_b , the bottom type is unchanged, except to bottom type 3a and 3b. This also

shows that it is possible there are one or no outer system (double-bars and plunging waves), the inner bottom profile only depends on breaking wave forcing. We can imagine series of several double-bars with many plunging waves, the inner bottom type is strongly controlled by inner breaking wave characteristics.

Some type 4 platforms are characterized by an unsteady state. This phenomenon appears for high energy fluxes ($F > 1.7$ W/m, Fig. 7) and strong values of incident wave height $H > 4.5$ cm. This unsteadiness is characterized by the sandbars alternatively moving seaward and shoreward. However, it is difficult to distinguish any tendency in unsteady profiles in the (F_b, ξ_b) plan (Fig. 14). This would mean that the unsteadiness is linked to the incident wave parameters compared to the breaking waves parameters, they are observed for strong values of wave energy flux F .

4.5. Morphological and hydrodynamical correlations

We now compare morphological and hydrodynamical singularities for bottom profiles presenting one (types 1, 2, 3a and 3b) then two (types 41, 42, 43a and 43b) systems. A schematic representation of these characteristics are represented in Figure 15.

One-system bottom types (1, 2, 3a and 3b)

For one-system bottom types, we observed that (B) and (S) corresponds to the location of the swash zone top x_{SWt} . Similarly, (PS) coincide with the breaker point x_b . Therefore, the platform length L_P is almost equal to the cumulated size of the surf and swash zones $L_P \approx L_{SF} + L_{SW}$. For all bottom types except 3a, the location of the limit of the surf zone to the swash zone x_{SWb} is related to (SC). The swash zone is located over the steep terrace of the inner platform. For the bottom type 3a, x_{SWb} is characterized by (SS), the inner platform is a gentle terrace and the swash zone is short and merges with the "concave" profile. Hence, the inner and outer platforms correspond to the swash $L_{Pi} \approx L_{SW}$ and surf $L_{Po} \approx L_{SF}$ zones respectively.

The surf zone can be subdivided in two parts, an outer surf zone where waves breaks and an inner surf zone where waves are transformed in propagating bore. We observed that the bottom types 1 and 2 are related to an only outer surf zone, contrary to the bottom types 3a and 3b where we see the both inner and outer surf zones. We estimated the position between these two parts from the photos of the bottom types (in Fig. 10 and 11), and it seems corresponds to (ZS).

Two-systems bottom types (41, 42, 43a and 43b)

For two-systems bottom types, (B) and (S) likewise corresponds to the location of the swash zone top x_{SWt} . x_{SWb} is related to (SS) for bottom type 43a and with (SC) for the others bottom types. (PS') coincide with the breaker point x_b and (PS) seems correspond to the secondary breaker point (cf Fig. 12). For all bottom types, we observed the both inner and outer surf zones (Fig. 12 (a)-(e)). The outer surf zone is delimited by (PS') and (ZS') and the inner surf zone by (ZS') and the bottom of the swash zone.

The total platform length L_P is also equal to the cumulated size of the surf and swash zones $L_P \approx L_{SF} + L_{SW}$. The inner platform defined from (PS) to (S) for two-systems bottom types corresponds to the outer platform of one-system bottom types.

5. Influence of granulometry and cliff height on bottom morphologies

The classification we propose has been established for a given grain size of sediment ($C41, D_{50} = 0.41$ mm) and a

given cliff height $h_C = 8$ cm. In order to study the system behavior for different sediment grain sizes and cliff heights, we used different sand types and we varied the cliff height.

5.1. Influence of grain diameter

We used two other sands: a finer S28 and a coarser S48 (D_{50} of, respectively, 0.28 and 0.48 mm). The two parameters F and ξ used above are not adapted to study the grain size effect because they only represent hydrodynamics. We therefore chose two hydro-sedimentary parameters, the Dean number Ω and the Shields number Θ . As for the Dean number Ω , the Shields number is calculated at the breaker (Θ_b). Thus, a figure of bottom typology in the (Ω, Θ_b) diagram is drawn for each sand type (Fig. 16). We observed the bottom typology strongly depends on Ω than Θ_b , but the dependency on Θ_b decreases with grain size. The three types of sand are similarly organized in terms of Shields number range: $\Theta_b < 0.15$ for the fine-grained sand (Fig. 16a), $\Theta_b < 0.22$ for the C41 sand (Fig. 16b) and $\Theta_b < 0.16$ for the coarse sand (Fig. 16c). This range of Shields number only corresponds to a bedload transport regime. By cons, an important difference in the range of Dean number can be observed (Fig. 16). For the coarser sand (S48), the boundaries are shifted to lower values of Ω compared to the other sands (C41 and S28): it ranges from 1 to 3 for the finest sand S28, while it ranges between 0.5 and 2.5 for C41 and S48. Whatever the grain size, we observe that the bottom types and morphologies are identical to those obtained for the sand C41. To explain this difference, we represent lateral photos of the same type of bottom morphology (type 2) for the three sand types in Figure 17. We observe that the bottom shape is similar for each sand, however we note the eroded sediment extends further seaward for the finer sand (Fig. 17). Indeed, the suspension of sediment is more important for fine-grained sediments, this implies ripples formation at the shoaling zone (Fig. 17a) and an erosion more important. We realised an experiment with a very fine sand ($D_{50} = 0.11$ mm) and we observed an important suspension close to the bottom, ripples over the entire platform and a strong erosion. This shows a transition towards a different bottom typology, the classification carried out in this study is robust for a some range of sediment grain size (0.28 mm $\leq D_{50} \leq 0.48$ mm).

5.2. Influence of cliff height

We now vary the cliff height h_C to know how it may affect the bottom morphodynamics. Indeed, for the same retreat rate the higher the cliff, the more voluminous the available sediment is. The type of the bottom morphology for different cliff heights is presented in the (F_b, ξ_b) diagram (Fig. 18). We can observe that a bottom morphology is of the same type for a given wave forcing (F_b, ξ_b) regardless of the cliff height. For example, $(F_b, \xi_b) \approx (2.8$ W/m, 0, 31) corresponds to a bottom morphology of type 42 for the different cliff heights, $h_C = 8$ cm (Fig. 18b), $h_C = 10$ cm (Fig. 18c), $h_C = 12$ cm (Fig. 18d) and $h_C = 15$ cm (Fig. 18e). In fact, the eroded volume of sediment is almost the same whatever the cliff height. Figure 19 shows the comparison of a same bottom type with a given incident wave forcing for different cliff heights. The bottom types compared are types 1 (Fig. 19a), 3b (Fig. 19b), 41 (Fig. 19c) and 42 (Fig. 19d). First, the bottom profiles are very similar for each case. We can observe in Figure 19b that the slope of inner platform is slightly lower for $h_C = 8$ cm (about 15%) than for the higher cliffs (about 20%). However, except this part of the profile, the bottom morphologies overlap very well for each case. Second, the cliff retreat is greater for a small cliff than for a high cliff for four cases. The cliff position for bottom types 1 and 3b are almost the same for $h_C = 8$ cm ($x_C \approx 21$ cm) and $h_C = 12$ cm ($x_C \approx 27 - 28$ cm). The wave energy

flux is almost equal $F \approx 1.1$ W/m while $\xi_b = 0.66 - 0.67$ and $\xi_b = 0.50 - 0.54$ for bottom types 1 and 3b respectively. This shows that the cliff retreat does not directly vary with ξ_b and therefore with bottom morphodynamics. Finally, the eroded volumes of sediment were estimated by integration of bottom profiles from the shoreline to seaward. For a given wave forcing, the eroded volumes are very close whatever the cliff height with a maximum difference reaching 14%. Otherwise, the wave forcing differs until about 10%. We also observed collapse volume increases with cliff height and so the volume of sediment injected in the system depends on the cliff height, this implies a shape change of cliff front. For instance, the sand profile of bottom type 3b (Fig. 19b) can present a notch for $h_C = 12$ cm, cliff debris for $h_C = 10$ cm and a vertical cliff for $h_C = 8$ cm. This reflects that the system is stabilised with a vertical cliff for an eroded volume $V_e = 262.7$ cm³/cm. For $h_C = 10$ cm, there is a surplus of injected sediment hence debris stay at the cliff bottom. For $h_C = 12$ cm, the notch formation shows a lack of sediment in the system, the eroded volume is slightly lower $V_e = 235.4$ cm³/cm than for the other cliff heights (Fig. 19b). Therefore, even if sediment is injected in the system, the eroded volume of sediment is fixed and controlled by a given wave forcing. However, we observed few cases with a same incident wave forcing which destabilize for an important eroded volume of sediment implying the existence of the unsteadiness of the bottom morphology.

6. Discussion

We identified four main bottom morphologies as a function of the shape of the outer platform, (i) steep terrace (type 1), (ii) one-bar profile (type 2), (iii) gentle terrace (type 3) and (iv) double-systems profile with two outer bars (type 4). We observed different types of breaking waves over the outer platform closely linked to bottom typology (surging, collapsing, spilling and plunging, respectively). Outer and inner platforms of one-system profiles (types 1, 2 and 3) correspond to the surf and swash zones respectively. The inner platform is either a large steep terrace (types 1, 2 and 3b) for strong wave energy flux or a small gentle terrace (type 3a) for low wave energy flux. Therefore for bottom type 3a, the swash zone is small for low energy flux and plunging/spilling breakers. This feature could be explained by the fact that the energy of wave front in the surf zone and so the runup are low, and large steep terraces would form for high runup energy. Type 4 morphologies present two sub-systems with two distinct breaking waves. The outer system is characterized by a double-bar profile and the inner system corresponds to a type 1, 2 or 3 profile (types 41, 42 and 43). We showed that the bottom typology depends more on the surf similarity parameter ξ than the incident wave energy flux F . Moreover, it better depends on the surf similarity parameter at the breaker point ξ_b .

This bottom classification is robust for some range of grain sizes. Indeed, ripples appearance decreases and erosion increases with grain size. We conclude that bottom types mainly depend on the Dean number Ω , and slightly on the Shields number Θ_b . The dependance on Θ_b appears to be more important for fine sand (S28) than for coarser sands (C41 and S48). The regime of sediment transport and eroded volume of sediment strongly controls the range of hydro-sedimentary parameters on the bottom typology.

The material choice was based on the representation of cliff recession and bottom morphology in the nature. The experiments carried out are representative of a soft cliff with a bottom typology for a low-energetic wave forcing. Unlike a natural beach where the sediment volume is limited, in a cliff/platform system the sediment volume is available from the collapse events of cliff retreat. Moreover, the feature of

our system is the sediment supply from the shore, that can be analog to a beach nourishment. That is to say, the system manages by itself the sediment flux in the morphological system.

[Wright and Short, 1984]’s classification shows that the threshold value of Dean number $\Omega = 1$ delimits the bottom profiles of “reflective” type and intermediate profiles. [Wright and Short, 1984] were observed “reflective” beach state is composed of steep beach face with surging breakers. In our study, type 1 profiles corresponds to the “reflective” profile, the threshold value of Dean number slightly changes for the different sediment grain size used, from $\Omega < 1.3$ for the finer sand (S28) to $\Omega < 0.8$ for C41 sand. The intermediate beach states observed by [Wright and Short, 1984] are (i) Ridge-Runnel or Low Tide Terrace (RRT or LTT), (ii) Transverse Bar and Rip (TBR), (iii) Rhythmic Bar and Beach (RBB) and (iv) Longshore Bar-Trough (LBT) for increasing Dean number Ω . Our type 2 profiles corresponds to the RRT beach state which is formed of a flat bar with plunging breakers, a runnel and a steep beach face. The type 3b profiles could correspond to LTT formed of terrace and steep beach face. TBR beach state varies alternatively in longshore direction in two states, the one similar to RRT with a very flat bar (almost a terrace) and the other formed of terrace with spilling/plunging breakers and a gentle beach face. The type 3b and 3a profiles, respectively, corresponds to these both states of the TBR beach state. RBB and LBT beach states are double-systems profiles with two breakers locations, as the type 4 profiles of our study. RBB beach state also varies in longshore direction in two states, the one with plunging breakers into an outer bar and surging breakers into steep beach face, and the other is formed of mega ripples. Hence, the type 41 profiles seem corresponds to the first state of RBB beach profile. Likewise, they could correspond to LBT beach state because it is formed of a bar with plunging breakers and a steep reflective beach face with surging breakers. Hence, types 2, 3 and 4 profiles corresponds to intermediate profiles ($1 < \Omega < 5$) of the [Wright and Short, 1984]’s classification. Natural bottom profiles with two distinct systems were classified by [Price and Ruessink, 2011] using the [Wright and Short, 1984]’s classification for each system. Similarly, the type 4 bottom profiles are classified by separating it in two sub-systems, the outer with a double-bars and the inner in type 1, 2 or 3 profile. Thus, we could study systems with multiple bars through characterization of each sub-system by knowing of the corresponding breaker wave parameters. [Makaske and Augustinus, 1998] have observed in the field steep, concave and convex-concave profiles for increasing wave height at breaker point H_b , i.e. for increasing F_b and decreasing ξ_b . Similarly, for increasing ξ_b , the type 1 profiles of our typology have a steep shape and the platform step of the types 2 (bared), 3 (terrace) and 4 (bared) profiles can be considered as having a convex shape.

[Grasso et al., 2009]’s observations from laboratory experiments show terraced profiles for $\Omega = 2.5$ and $\Omega = 3.7$, the outer platform is a gentle terrace and the inner platform is a steep terrace. The type 3b profiles of our classification corresponds to the first bottom type ($\Omega = 2.5$) because [Grasso et al., 2009] observed spilling breakers at the outer platform. We observed this bottom type for $0.8 \leq \Omega \leq 2$ depending on grain size of sediment, this difference is explained by the use of lightweight sediment by [Grasso et al., 2009]. For the second bottom type ($\Omega = 3.7$), breakers have been observed at the inner platform, this could be explained by the generation of irregular waves which tend to flatten the bottom profile. Indeed, the generation of regular waves involves the same breakers position and the possible formation of bars.

Therefore, our bottom typology seems consistent with different classifications of natural and laboratory bottom morphologies. Observed bottom types in this study and in the literature present similarly the same tendency as a function of wave forcing and sediment grain size.

Unsteady type 4 bottom profiles have been observed for $F > 1.7 W/m$. This instability is characterized by a temporal oscillation of sandbars and could be due to eigen modes of the system. However, beaches in England and Wales have been observed and classified by [Scott et al., 2011] as a function of wave and tide forcing based on the [Wright and Short, 1984]’s and [Masselink and Short, 1993]’s classifications. They determined a threshold value for wave energy flux ($F = 3 kW/m$) which separates intermediate beaches with ($F > 3 kW/m$) and without ($F < 3 kW/m$) three-dimensional bar/rip morphology. Unsteady profiles of our study could also be explained by the mark of this process. As experiments are confined in the transversal direction, a spatial unsteadiness would result by a temporal unsteadiness.

The bottom typology established is independent on the available sediment volume in the system, through the cliff height. However, the collapse volume, and so the injected sediment in the system, increases with the cliff height. We showed the eroded volume of sediment is almost constant for a given wave forcing whatever the cliff height, even if few bottom profiles destabilize for an important eroded volume leading to an unsteady state. Consequently, the conservation of the total volume of sediment in the system implies that the cliff retreat decreases with cliff height. Cliff retreat is not directly linked to the surf similarity parameter ξ , it shall depends on it, and so on the bottom type, as a non-monotonous function.

7. Conclusions

Experiments of sandy cliff erosion by waves have been carried out in a wave flume with a monochromatic wave forcing. We analysed different bottom morphology as a function of incident wave forcing (ξ, F) and wave parameters at the breaker point (ξ_b, F_b). A methodology of characterisation of bottom topography has been proposed. Our results show that the bottom type mainly depends on the surf similarity parameter rather than the wave energy flux. We showed that this characterisation is more relevant if we consider the wave height at the breaker point compared to the incident wave height offshore. For $D_{50} = 0.41 mm$, steep terraces with surging breaking waves are observed for $\xi_b > 0.48$, one-bared profiles with collapsing breaking waves for $0.42 < \xi_b < 0.48$, gentle terraces with spilling breaking waves for $0.38 < \xi_b < 0.43$ and two sub-systems profiles for $\xi_b < 0.38$ with two distinct types of breaking waves. These two sub-systems profiles are composed of a double-bars profile with a plunging breaking waves as the outer system and one of the three one-system defined previously as the inner system.

The bottom typology is robust for some range of the sediment grain size. The bottom type is more dependent on the Dean parameter than the Shields number at the breaker point. The ranges of these parameters of the four main bottom types is slightly different according to the grain diameter. Our classification is consistent with the ones of the literature on the beaches in the nature and in the laboratory. The bottom typology is not varied by the available sediment volume change and the cliff recession decreases with the cliff height. The cliff recession is not a monotonic function of the surf similarity parameter, it strongly depends on the bottom type. The eroded sediment volume is the same for a given wave forcing, however it seems play a role on the unsteadiness of the bottom morphology, so a reflection on its role could be developed regarding the beach nourishment projects. The volume of the injected sediment in the system is an important parameter to take into account for the knowledge of bottom dynamics, and in turn the cliff retreat is linked to the bottom type and hydrodynamics associated.

Acknowledgments. We gratefully acknowledge PRES Université de Toulouse for its financial support, as well as Institut National des Sciences de l'Univers (INSU) and SHOM ("Reliefs de la Terre program"), for additional funding of the Rocky cliff erosion project led by V.R. We also thank Serge Font, Sébastien Cazin and Herve Ayrolles for valuable technical assistance.

References

- Andrews, C., Williams, R. B. G. (2010), Limpet erosion of chalk shore platforms in southeast England, *Earth Surface Processes and Landforms*, 25, 1371–1381.
- Baldock, T., Manoonvoravong, P., Pham, K. (2010), Sediment transport and beach morphodynamics induced by free long waves, bound long waves and wave groups, *Coastal Engineering*, 57, 898–916.
- Brossard, J., Duperret, A. (2004), Coastal chalk cliff erosion: experimental investigation on the role of marine factors, *Coastal Chalk Cliff Instability, Geological Society, London, Engineering Geology Special Publications*, 20, 109–120.
- Caplain, B., Astruc, D., Regard, V., Moulin, F.Y. (2011), Cliff retreat and sea bed morphology under monochromatic wave forcing: Experimental study, *C.R. Geosciences*, 343, 471–477.
- Costa, S., Delahaye, D., Freiré-Díaz, S., Davidson, R., Di Nocera, L., Plessis Brossard, E. (2004), Quantification of the Normandy and Picardy chalk cliff retreat by photogrammetric analysis, *Coastal Chalk Cliff Instability, Geological Society, London, Engineering Geology Special Publications*, 20, 139–148.
- Damgaard, J. S., Dong, P. (2004), Soft cliff recession under oblique waves: physical model tests, *Journal of waterway, port, coastal and ocean engineering*, 130 (5), 234–242.
- Duperret, A., Genter, A., Delacourt, B., Mortimore, R. N., De Pomerai, M. (2002), Coastal rock cliff erosion by collapse at Puys (France) : the role of impervious marl seams within chalk of NW Europe, *Journal of Coastal Research*, 18, 52–61.
- Duperret, A., Genter, A., Martinez, A., Mortimore, R. N. (2004), Coastal chalk cliff instability in NW France: role of lithology, fracture pattern and rainfall, *Coastal Chalk Cliff Instability, Geological Society, London, Engineering Geology Special Publications*, 20, 33–55.
- Emery, K., Kuhn, G. (1980), Sea cliffs: their processes, profiles, and classification, *Geol. Soc. Am. Bull.*, 93, 644–654.
- Erikson, L., Larson, M., Hanson, H. (2007), Laboratory investigation of beach scarp and dune recession due to notching and subsequent failure, *Marine Geology*, 245, 1–19.
- Gallagher, E.L., Elgar, S., Guza, R.T. (1998), Observations of sand bar evolution on a natural beach, *Journal of Geophysical Research*, 103, 3203–3215.
- Grasso, F., Michallet, H., Barthélemy, E., Certain, R. (2009), Physical modeling of intermediate cross-shore beach morphology: Transients and equilibrium states, *Journal of Geophysical Research*, 114.
- Hampton, M. (2002), Gravitational Failure of Sea Cliffs in Weakly Lithified Sediment, *Environmental and Engineering Geoscience*, 8, 175–191.
- Hansom, J., Barltrop, N., Hall, A. (2008), Modelling the processes of cliff-top erosion and deposition under extreme storm waves, *Marine Geology*, 253, 36–50.
- Hegge, B., Eliot, I., Hsu, J. (1996), Sheltered Sandy Beaches of Southwestern Australia, *Journal of Coastal Research*, 12, 748–760.
- Kamalinezhad, M. (2004), Plages en équilibre morphologique et hydrodynamique associée, *Institut National Polytechnique de Grenoble (France)*.
- Kanyaya, J., Trenhaile, A. (2005), Tidal wetting and drying on shore platforms: an experimental assessment, *Geomorphology*, 70, 129–146.
- Kogure, T., Aoki, H., Maekado, A., Hirose, T., Matsukura, Y. (2006), Effect of the development of notches and tension cracks on instability of limestone coastal cliffs in the Ryukyus, Japan, *Geomorphology*, 80, 236–244.
- de Lange, W., Moon, V. (2005), Estimating long-term cliff recession rates from shore platform widths, *Engineering Geology*, 80, 292–301.
- Larson, M., Sunamura, T., Erikson, L., Bayram, A., Hanson, H. (2010), An analytical model to predict dune and cliff notching due to wave impact, *32nd Conference on Coastal Engineering, Shanghai, China, ASCE*.
- Le Roux, J.P. (2010), Sediment entrainment under fully developed waves as a function of water depth, boundary layer thickness, bottom slope and roughness, *Sedimentary Geology*, 223, 143–149, doi:10.1016/j.sedgeo.2009.11.006.
- Makaske, B., Augustinus, G. (1998), Morphologic Changes of a Micro-Tidal, Low Wave Energy Beach Face during a Spring-Neap Tide Cycle, Rhone-Delta, France, *Journal of Coastal Research*, 14, 632–645.
- Mansard, E., Funke, E. (1980), The Measurement of Incident and Reflected Spectra Using a Least Squares Method, *17th International Conference on Coastal Engineering, Sydney, ASCE*, 154–172.
- Masselink, G., Short, A. (1993), The effect of tide range on beach morphodynamics and morphology; a conceptual beach model, *Journal of Coastal Research*, 9, 785–800.
- Nesteroff, W., Mélières, F. (1967), L'érosion littorale du pays de Caux, *Bull. Soc. Geol. Fr*, 7, 159–169.
- Pierre, G. (2006), Processes and rate of retreat of the clay and sandstone sea cliffs of the northern Boulonnais (France), *Geomorphology*, 73, 64–77.
- Price, T., Ruessink, B. (2011), State dynamics of a double sand-bar system *Continental Shelf Research*, 31, 659–674.
- Ruessink, B., Wijnberg, K., Holman, R., Kuriyama, Y., van Enckevort, I. (2003), Intersite comparison of interannual nearshore bar behavior, *Journal of Geophysical Research*, 108.
- Sanders, N. (1968), Wave tank experiments on the erosion of rocky coasts, *Papers and Proceedings of the Royal Society of Tasmania*, 102, 11–16.
- Scott, T., Masselink, G., Russell, P. (2011), Morphodynamic characteristics and classification of beaches in England and Wales, *Marine Geology*, 286, 1–20.
- Stephenson, W. J., Kirk, R. M. (2000), Development of shore platforms on Kaikoura Peninsula, South Island, New Zealand - Part one: The role of waves, *Geomorphology*, 32, 21–41.
- Sunamura, T. (1992), *Geomorphology of Rocky Coasts, Wiley, New York*.
- Trenhaile, A. S. (2000), Modeling the development of wave-cut shore platforms, *Marine Geology*, 166, 163–178.
- Walkden, M., Dickson, M. (2008), Equilibrium erosion of soft rock shores with a shallow or absent beach under increased sea level rise, *Marine Geology*, 251, 75–84.
- Wang, T., Kraus, N. (2005), Beach profile equilibrium and patterns of wave decay and energy dissipation across the surf zone elucidated in a large-scale laboratory experiment, *Journal of Coastal Research*, 21, 522–534.
- Wolters, G., Muller, G. (2008), Effect of Cliff Shape on Internal Stresses and Rock Slope Stability, *Journal of Coastal Research*, 241, 43–50.
- Wright, L.D., Short, A.D. (1984), Morphodynamic variability of surf zones and beaches: A synthesis, *Marine Geology*, 56, 93–118.
- Young, A., Ashford, S. (2008), Instability investigation of cantilevered seacliffs, *Earth Surface Processes and Landforms*, 33, 1661–1677.
- Young, A., Guza, R., Flick, R., O'Reilly, W., Gutierrez, R. (2009), Rain, waves, and short-term evolution of composite seacliffs in southern California, *Marine Geology*, 267, 1–7.

B. Caplain, Université de Toulouse ;INPT, UPS; CNRS; IMFT, allée Camille Soula, F-31400 Toulouse, France. (caplain-bastien@gmail.com)

V. Regard, Université de Toulouse; UPS (OMP); CNRS; IRD; GET; 14 avenue Edouard Belin, F-31400 Toulouse, France.

D. Astruc, Université de Toulouse ;INPT, UPS; CNRS; IMFT, allée Camille Soula, F-31400 Toulouse, France.

Table 2. Sand characteristics.

Sand	Nature	Median diameter D_{50} (mm)	Density ρ_s (g/cm^3)	Fall velocity w_s (cm/s)
C41	Calcite	0.41	2.76	5.45
S28	Silice	0.28	2.65	3.24
S48	Silice	0.48	2.65	6.04

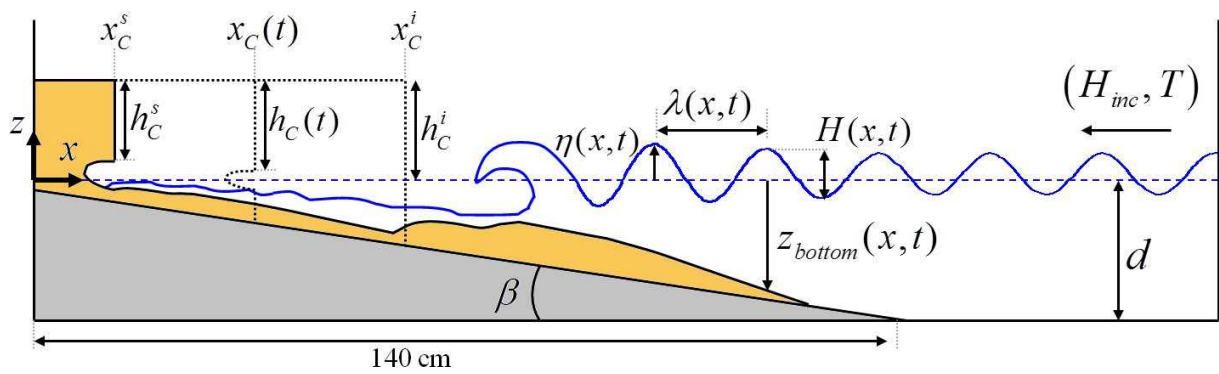


Figure 1. Schematic wave flume. h_C is the cliff height from the water surface at rest, x_C is the initial cliff position, β is the bottom rigid angle and d is the water depth. The (x, z) plan origin is located at the water surface and at the shoreward flume edge.

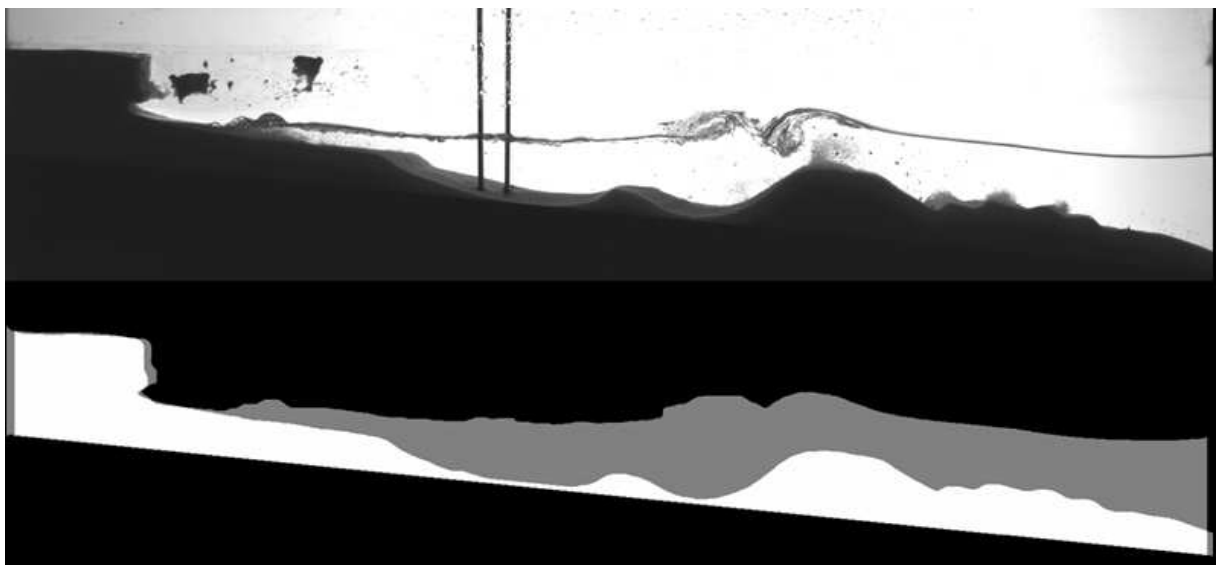


Figure 2. Raw image (up) and corresponding contours of sand surface and water free surface detected (down).

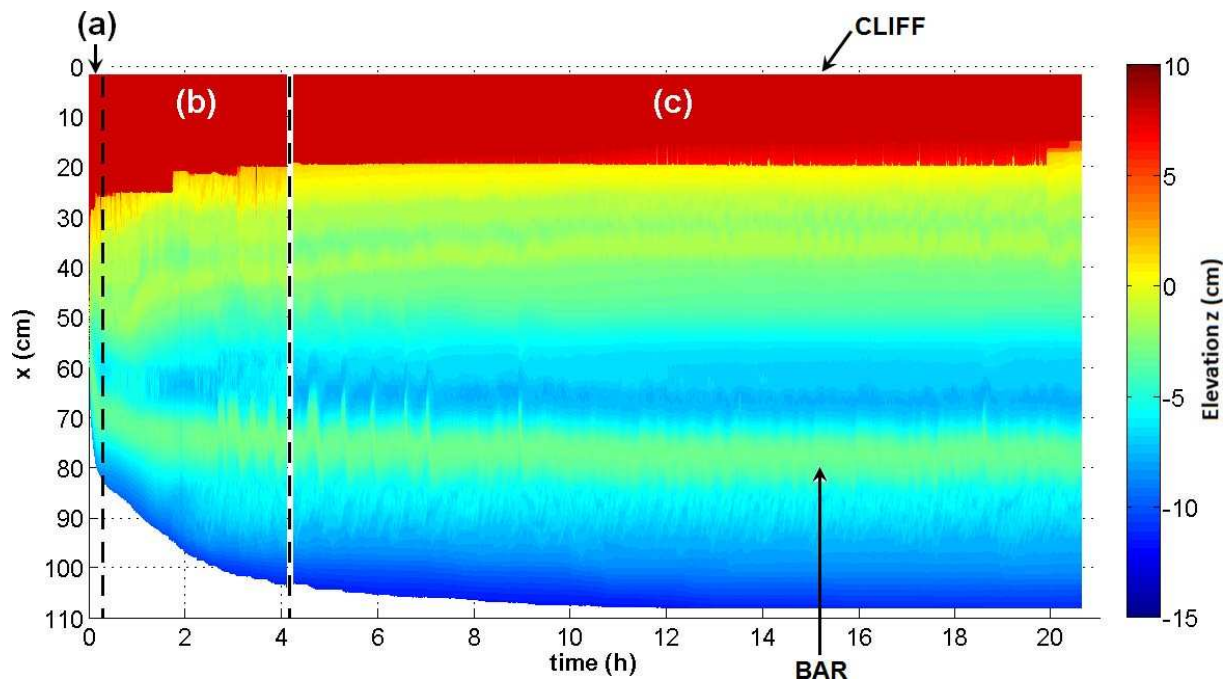


Figure 3. Spatial (x) and temporal (t) evolution of cliff and bottom morphology ($((F, \xi) = (1.2 \text{ W/m}; 0.39)$ case)). Color range indicates the sand surface elevation. Dashed lines separate the three phases of the experiment: (a) initiation, (b) transient and (c) stabilization.

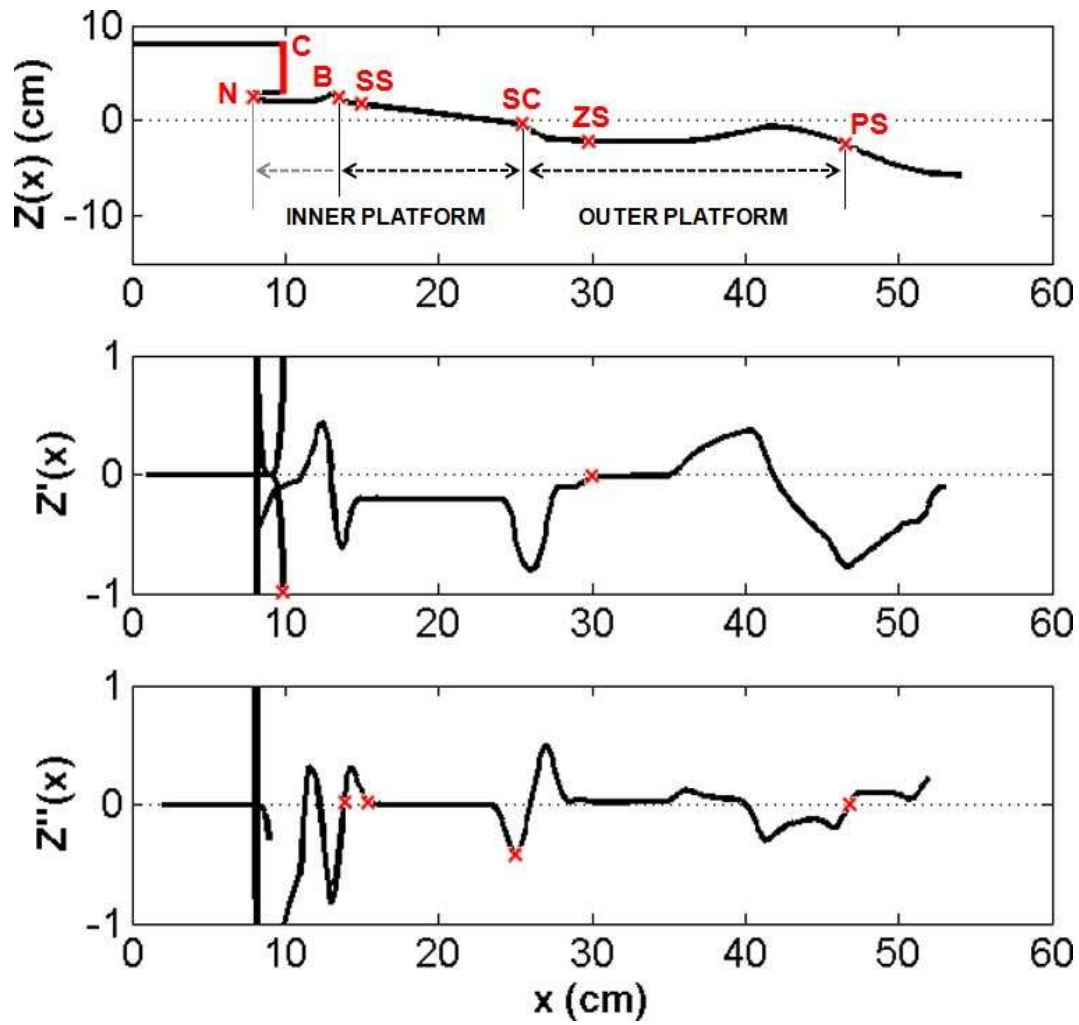


Figure 4. Schematic representation of sand surface profile $Z(x)$ and its first $Z'(x)$ and second $Z''(x)$ derivatives. (N), (C), (B), (CC), (SC), (ZS) and (PS) are the morphological singularities identified.

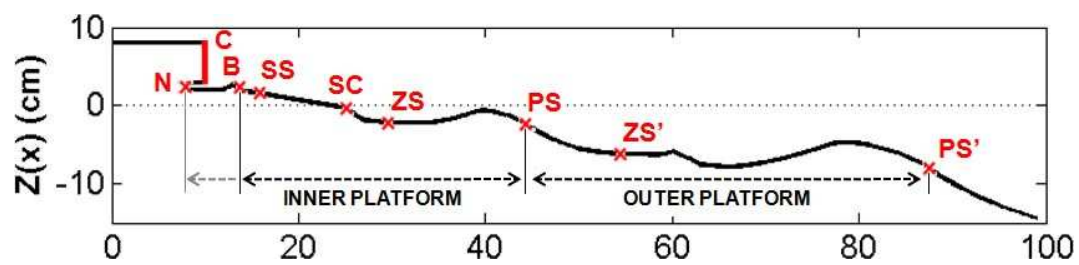


Figure 5. Schematic representation of sand surface profile $Z(x)$ for two-systems bottom profiles. (N), (C), (B), (CC), (SC), (ZS), (PS), (ZS') and (PS') are the morphological singularities identified.

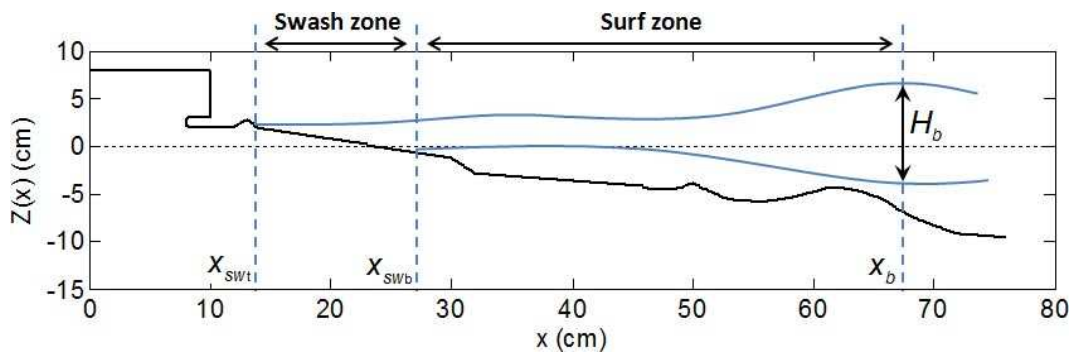


Figure 6. Schematic representation of sand surface profile and wave envelope. It allows to introduce hydrodynamical parameters: H_b is the wave height at the breaker point, x_b is the breaker point abscisse, x_{SW} is the abscisse of the swash zone bottom and x_{SL} is the shoreline abscisse corresponding to the swash zone top.

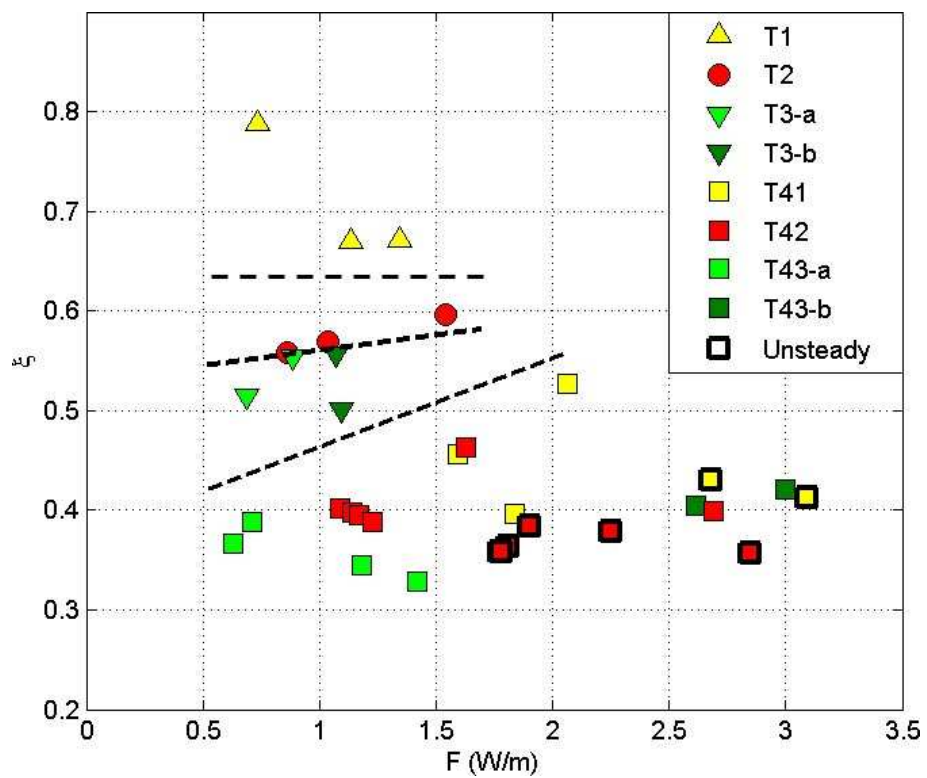


Figure 7. Diagram of bottom typology as a function of wave parameters (F, ξ). See text for the classification from T1 to T43b.

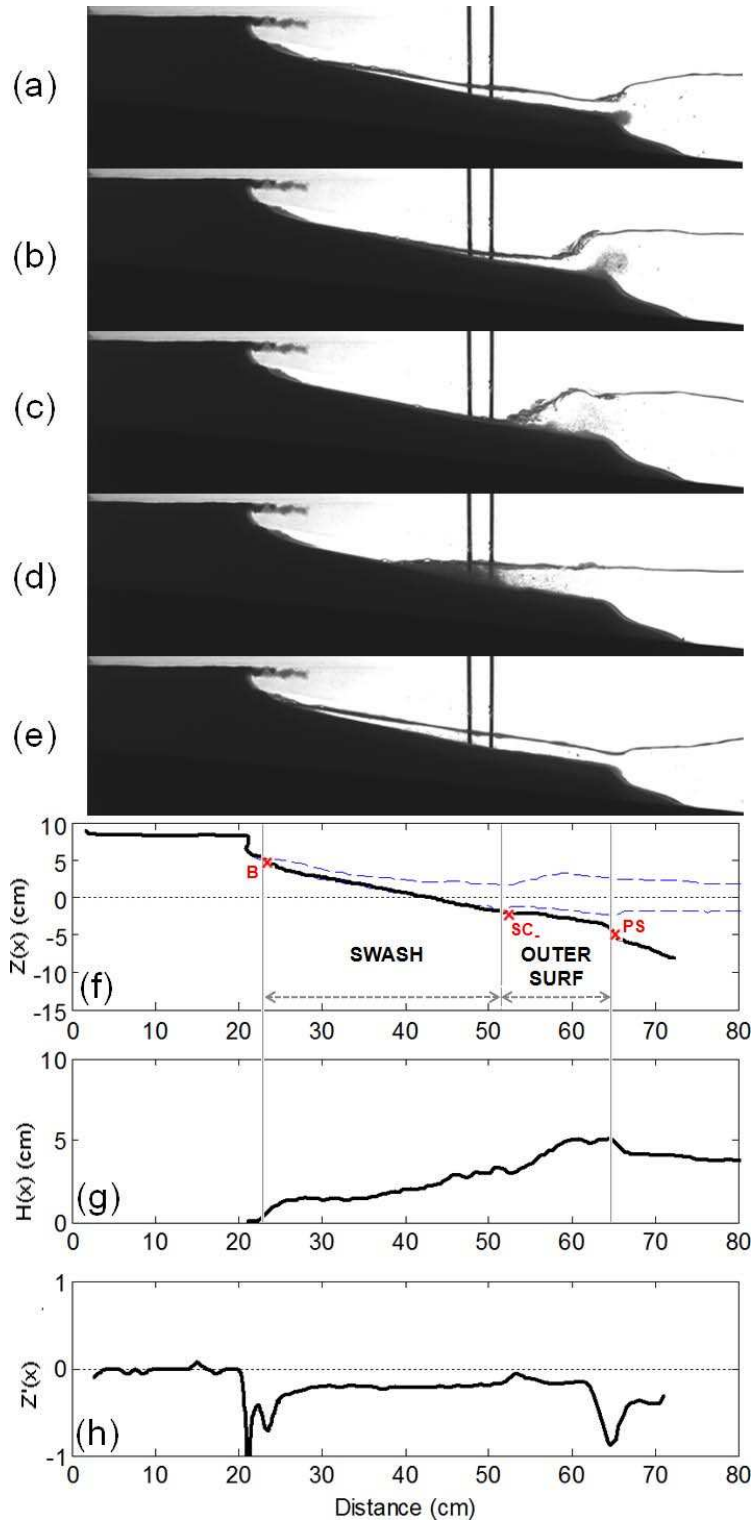


Figure 8. Bottom type 1 where $(F, \xi) = (1.1 W/m, 0.67)$. (a)-(b)-(c)-(d)-(e) lateral visualisation, (f) time-averaged bottom and cliff profiles $Z(x)$ and wave envelope, (g) wave height $H(x)$, (h) first derivative of sand profile $Z'(x)$.

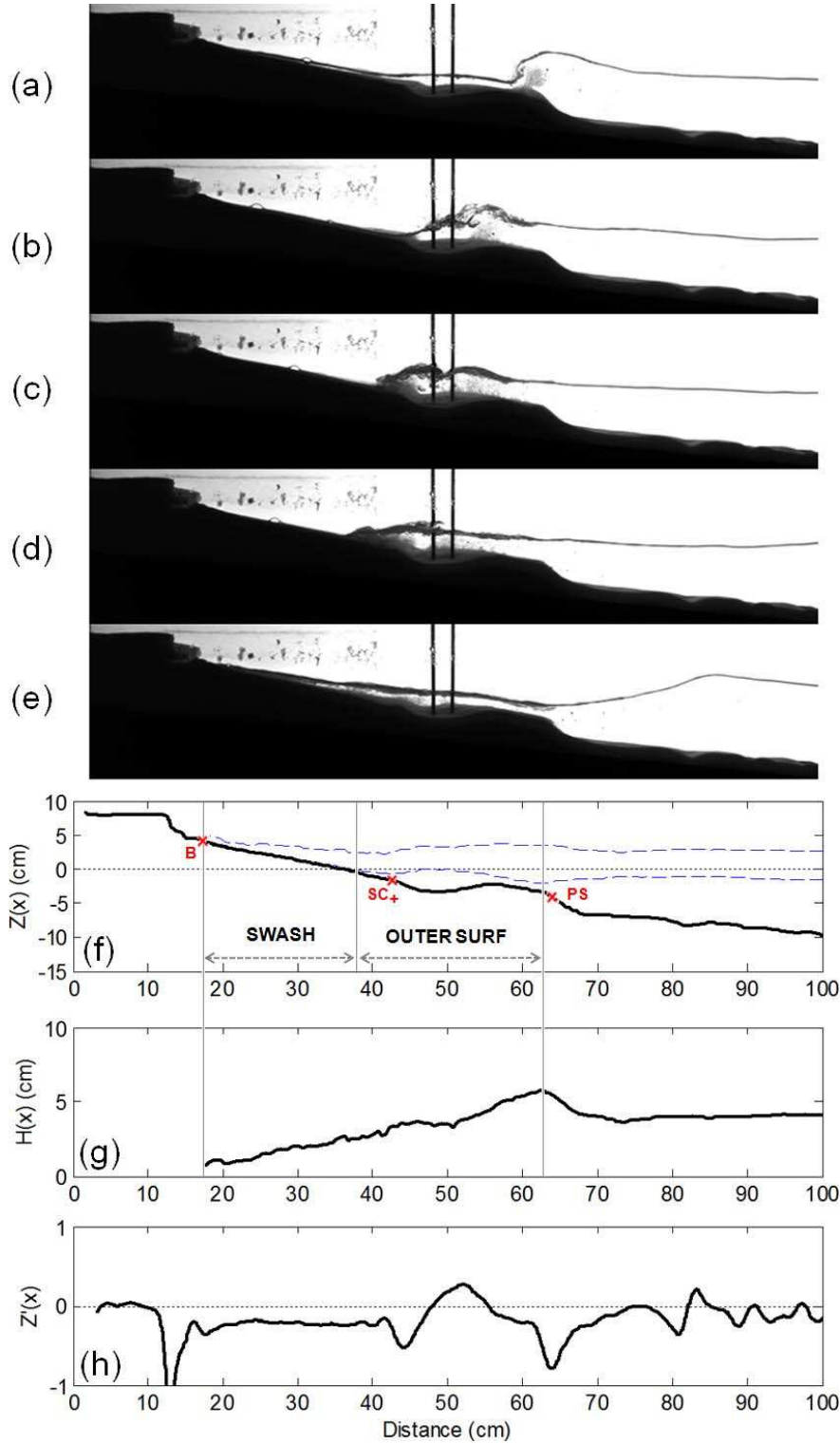


Figure 9. Bottom type 2 where $(F, \xi) = (1.0 W/m, 0.57)$. Same legend as Figure 8.

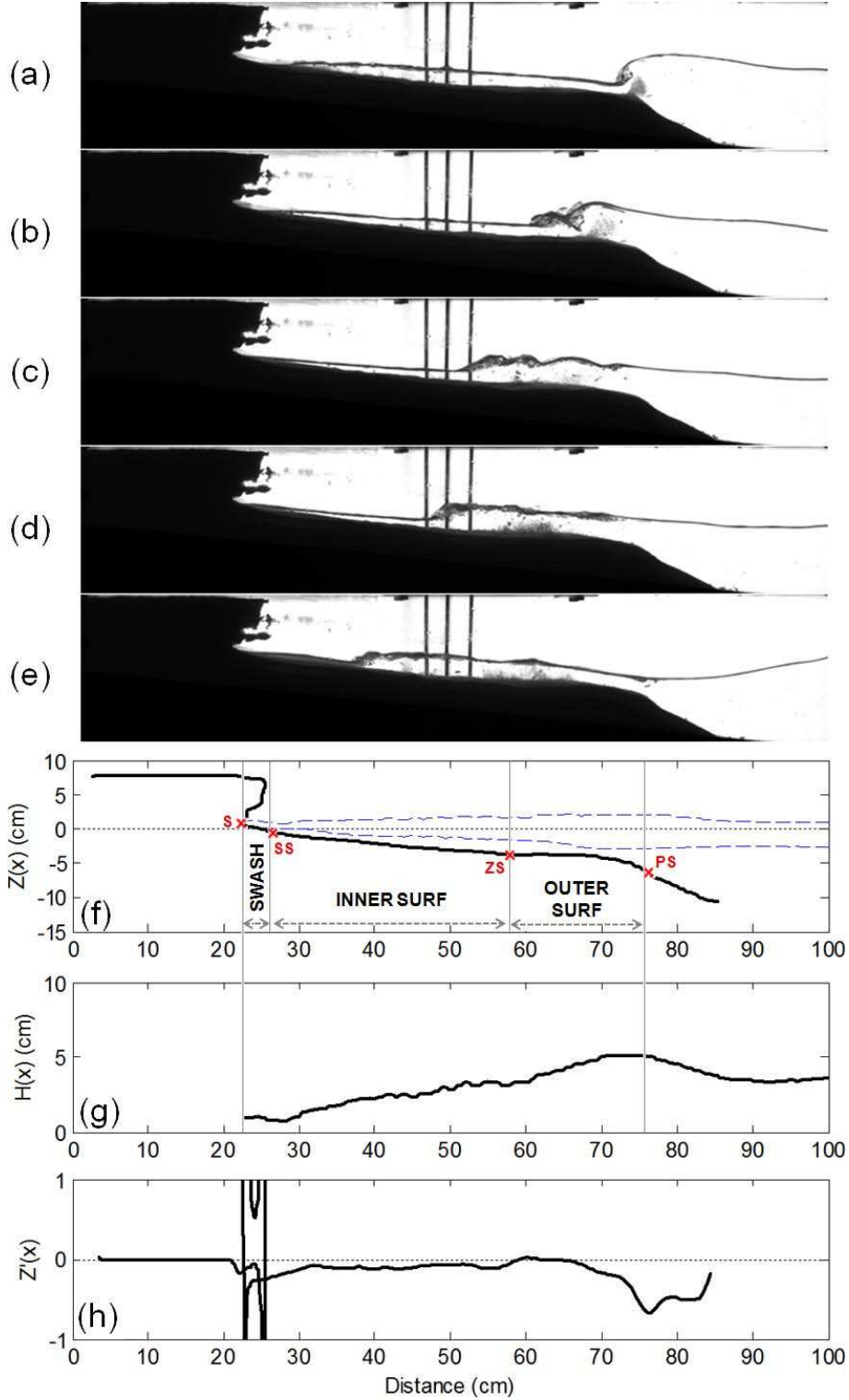


Figure 10. Bottom type 3a where $(F, \xi) = (0.9 W/m, 0.55)$. Same legend as Figure 8.

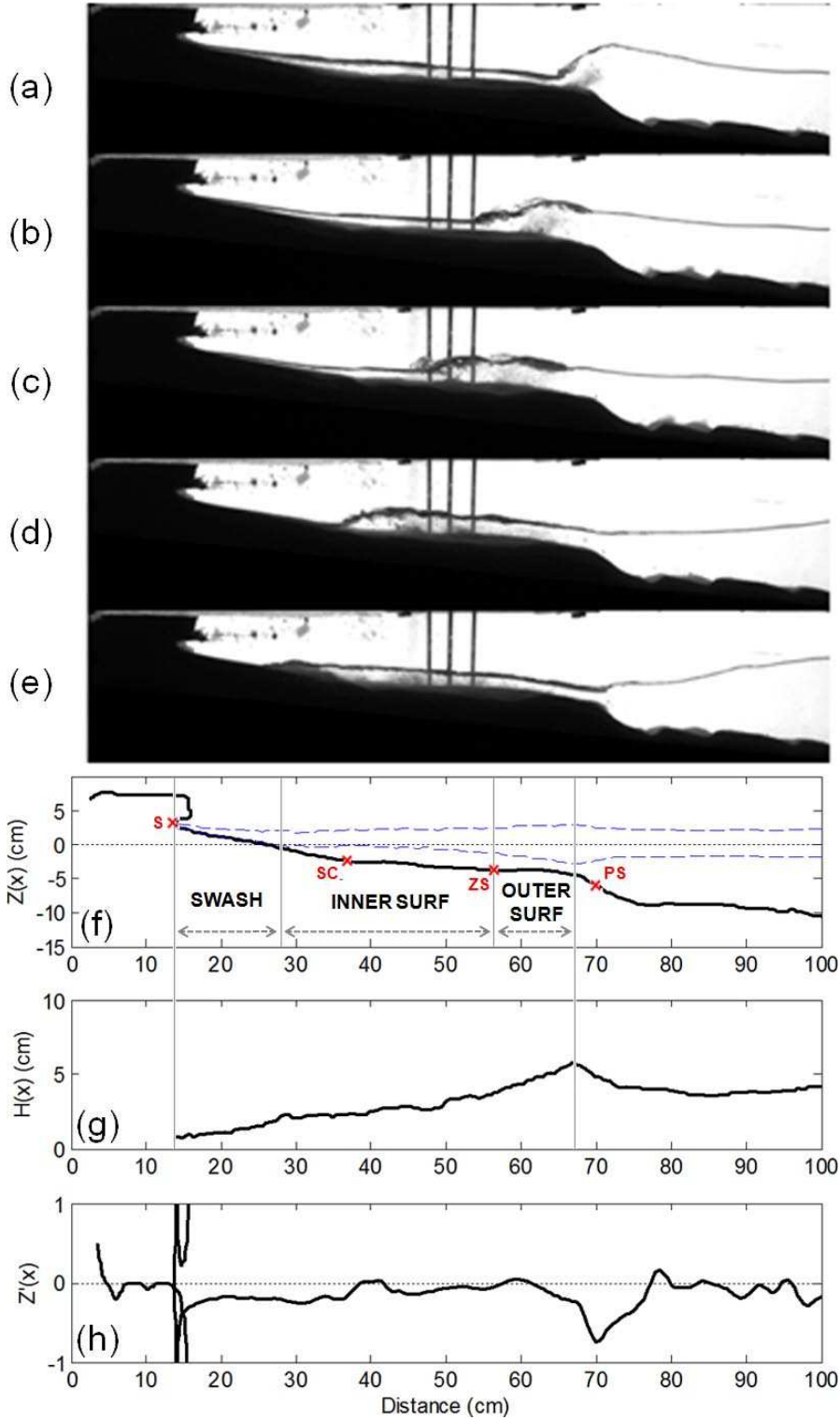


Figure 11. Bottom type 3b where $(F, \xi) = (1.1 W/m, 0.56)$. Same legend as Figure 8.

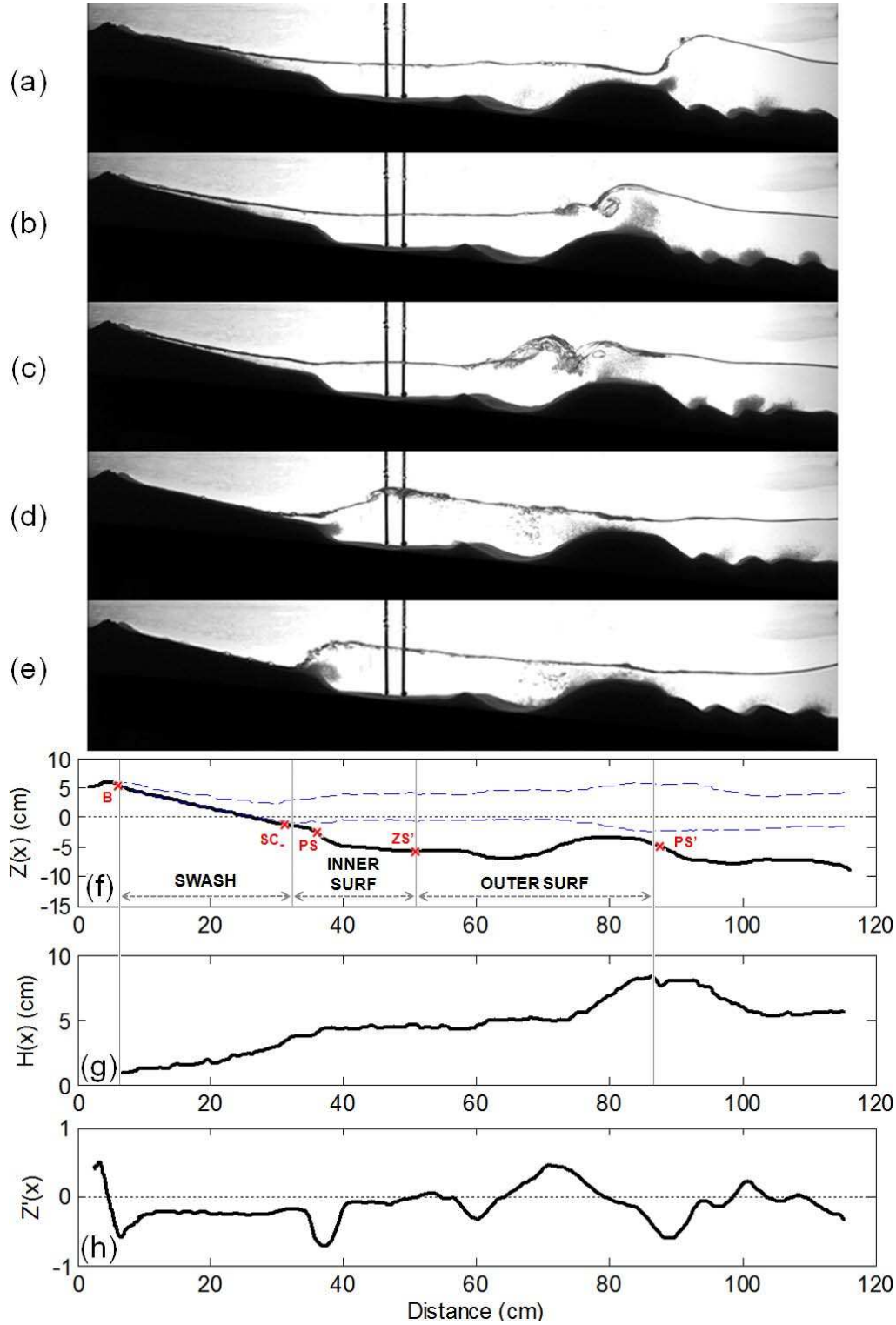


Figure 12. Bottom type 41 where $(F, \xi) = (2.1 W/m, 0.53)$. Same legend as Figure 8.

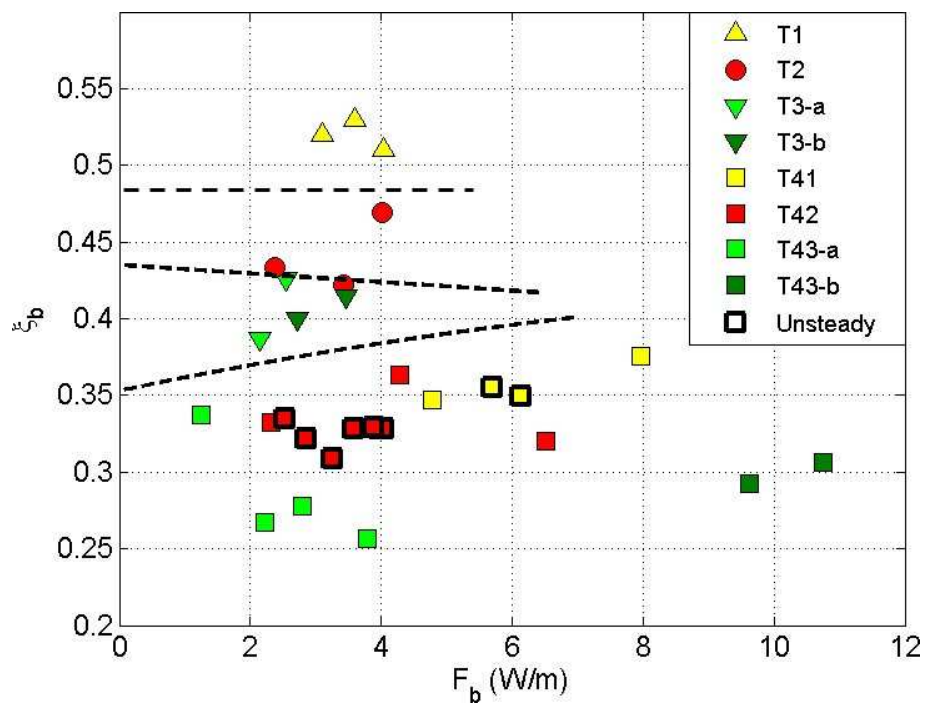


Figure 13. Diagram of bottom typology as a function of wave parameters at the breaker point (F_b, ξ_b). Curves which connect two symbols represent unsteady cases with oscillating bars. These two symbols correspond to wave forcing of two outer bar positions.

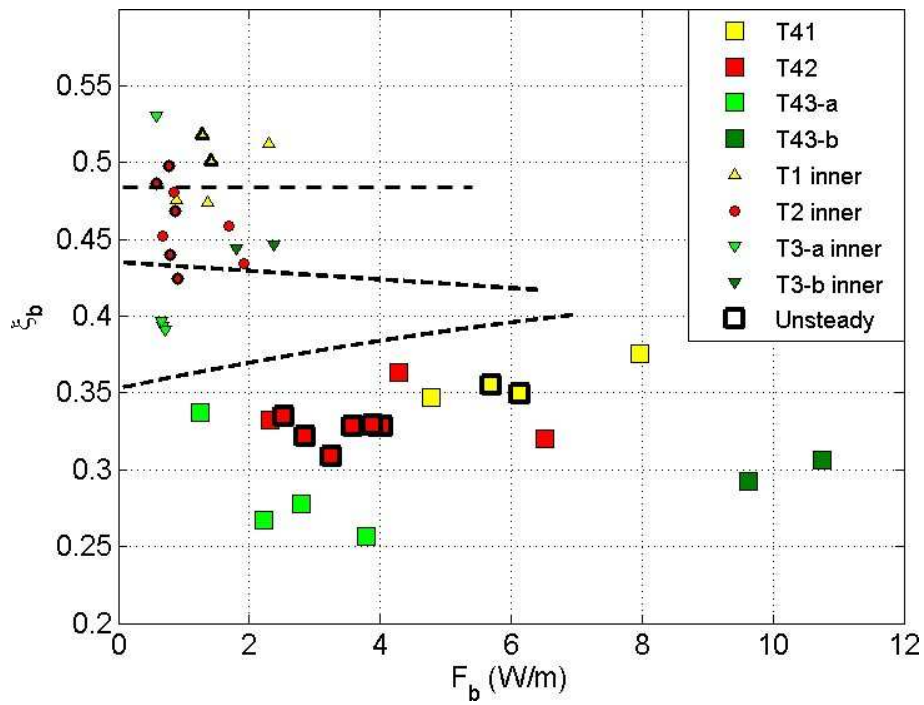


Figure 14. Diagram of bottom type 4 as a function of wave parameters at the breaker point (F_b, ξ_b) . Small symbols correspond to the waves parameters at the inner system of bottom type 4.

Table 1. Characteristics of bottom typology.

Bottom Typology	Outer Platform	Inner Platform	Sequence of Morphological Singularities	Swash zone length L_{SW}	Breaking wave type	L_P/λ	Incident wave forcing (F, ξ)	Breaking wave forcing (F_b, ξ_b)
1	Steep Terrace	Steep Terrace	$\{(B) - (SC_-) - (PS)\}$	$\sim L_{Pi}$	Surging	~ 0.30	$\xi \geq 0.65$	$\xi_b \geq 0.48$
2	Bared	Steep Terrace	$\{(B) - (SC_+) - (PS)\}$	$\sim L_{Pi}$	Collapsing	$\sim 0.40 - 0.45$	$0.55 \leq \xi \leq 0.6$	$0.42 \leq \xi_b \leq 0.48$
3	Gentle Terrace	Gentle Terrace	$\{(S) - (SS) - (ZS) - (PS)\}$	$\sim L_C$	Spilling	$\sim 0.55 - 0.6$	$F < 0.7 \text{ W/m}$ $0.5 \leq \xi \leq 0.55$ $1 \text{ W/m} \leq F \leq 1.3 \text{ W/m}$ $0.5 \leq \xi \leq 0.55$	$0.38 \leq \xi_b \leq 0.43$
		Steep Terrace	$\{(S) - (SC) - (ZS) - (PS)\}$	$\sim L_{Pi}$				
4	Breaker bar and splash-up bar	Type 1, 2, 3a or 3b	$\{(Sequence\ of\ inner\ bottom\ type\ 1,\ 2\ or\ 3) - (ZS') - (PS')\}$		Plunging	≥ 1	$\xi \leq 0.5$ and $(F, \xi) = (2.1 \text{ W/m}, 0.53)$	$\xi_b \leq 0.38$

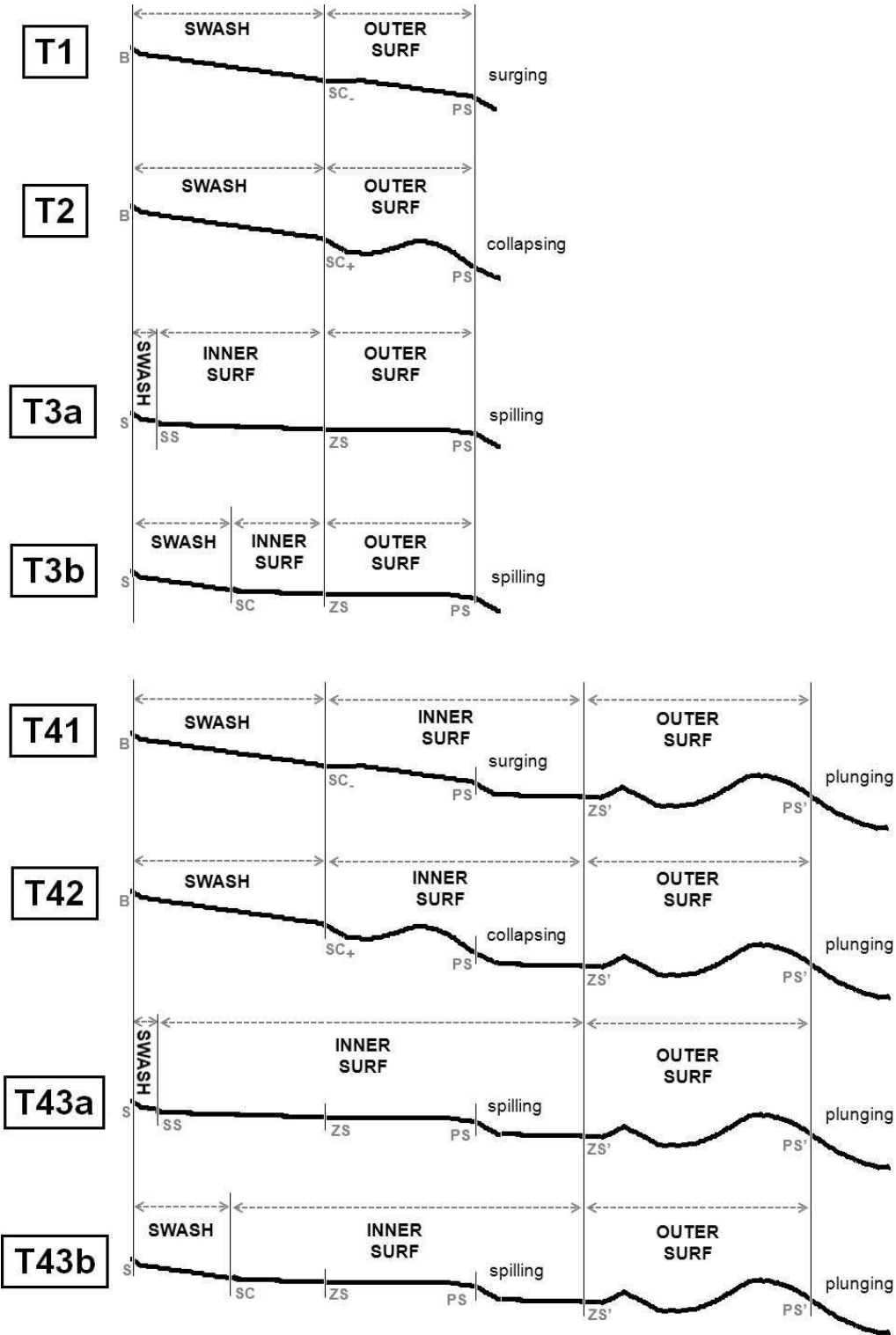
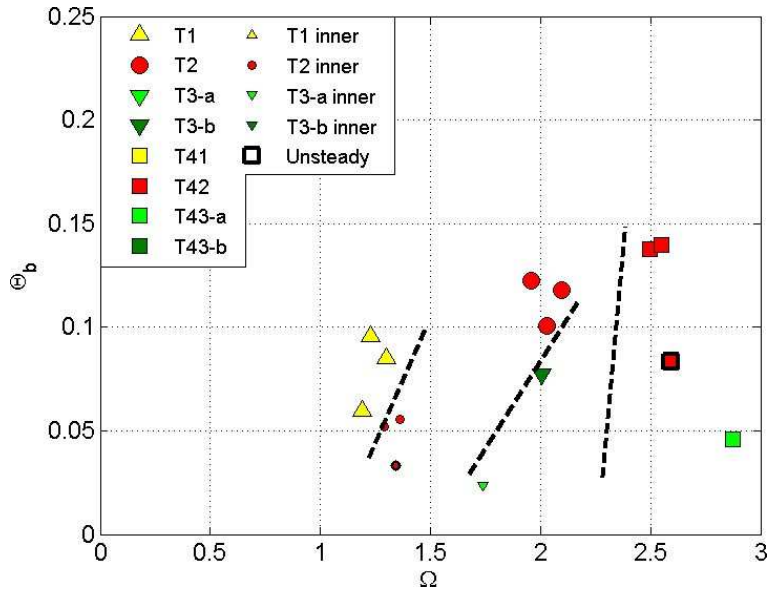
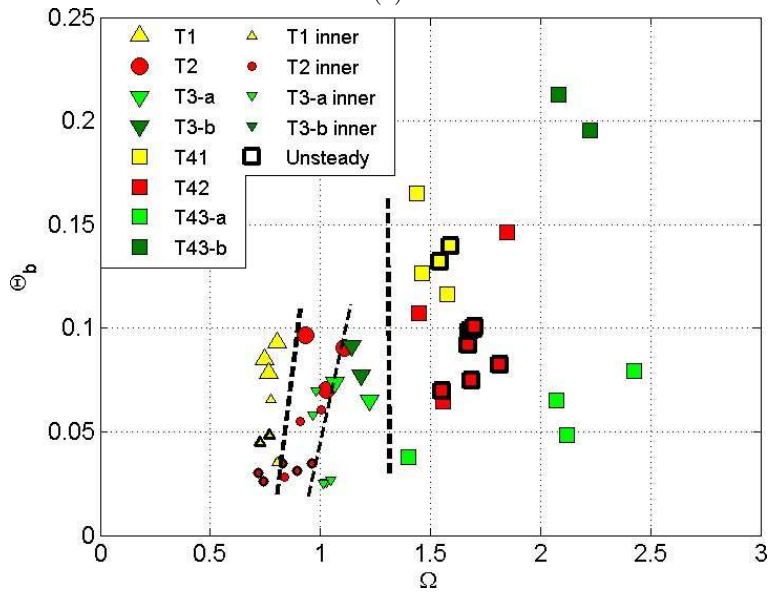


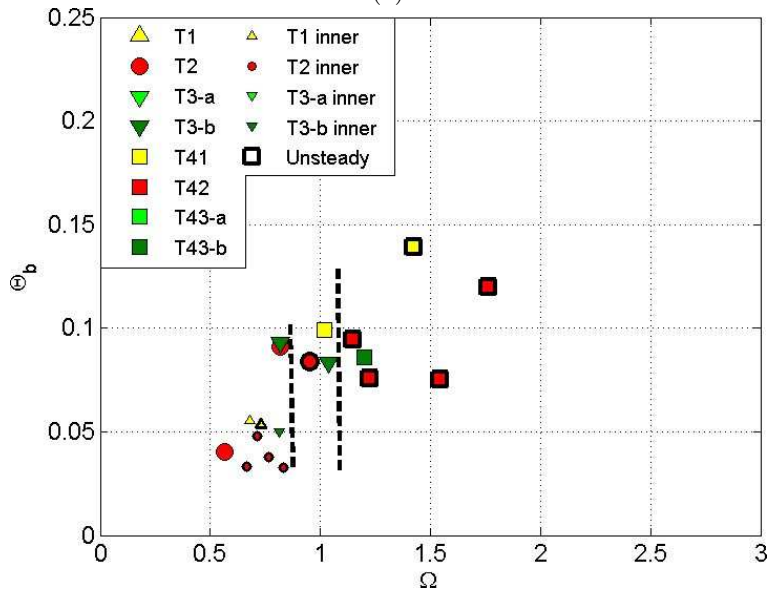
Figure 15. Schematic typology of observed bottom profiles.



(a)



(b)



(c)

Figure 16. Diagram of bottom typology as a function of (Ω, Θ_b) for different sand types : (a) S28, (b) C41, (c) S48. Representation of symbols are the same as Figure 14.

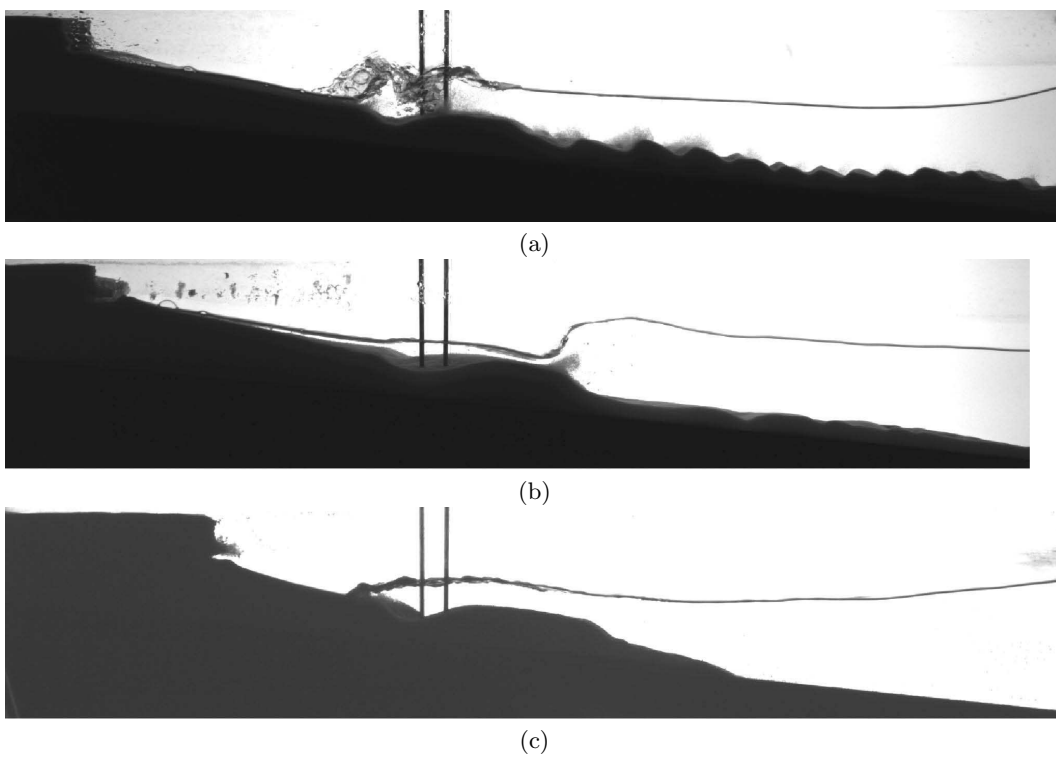


Figure 17. Lateral photos of bottom type 2 for three grain sizes: (a) S28, (b) C41, (c) S48.

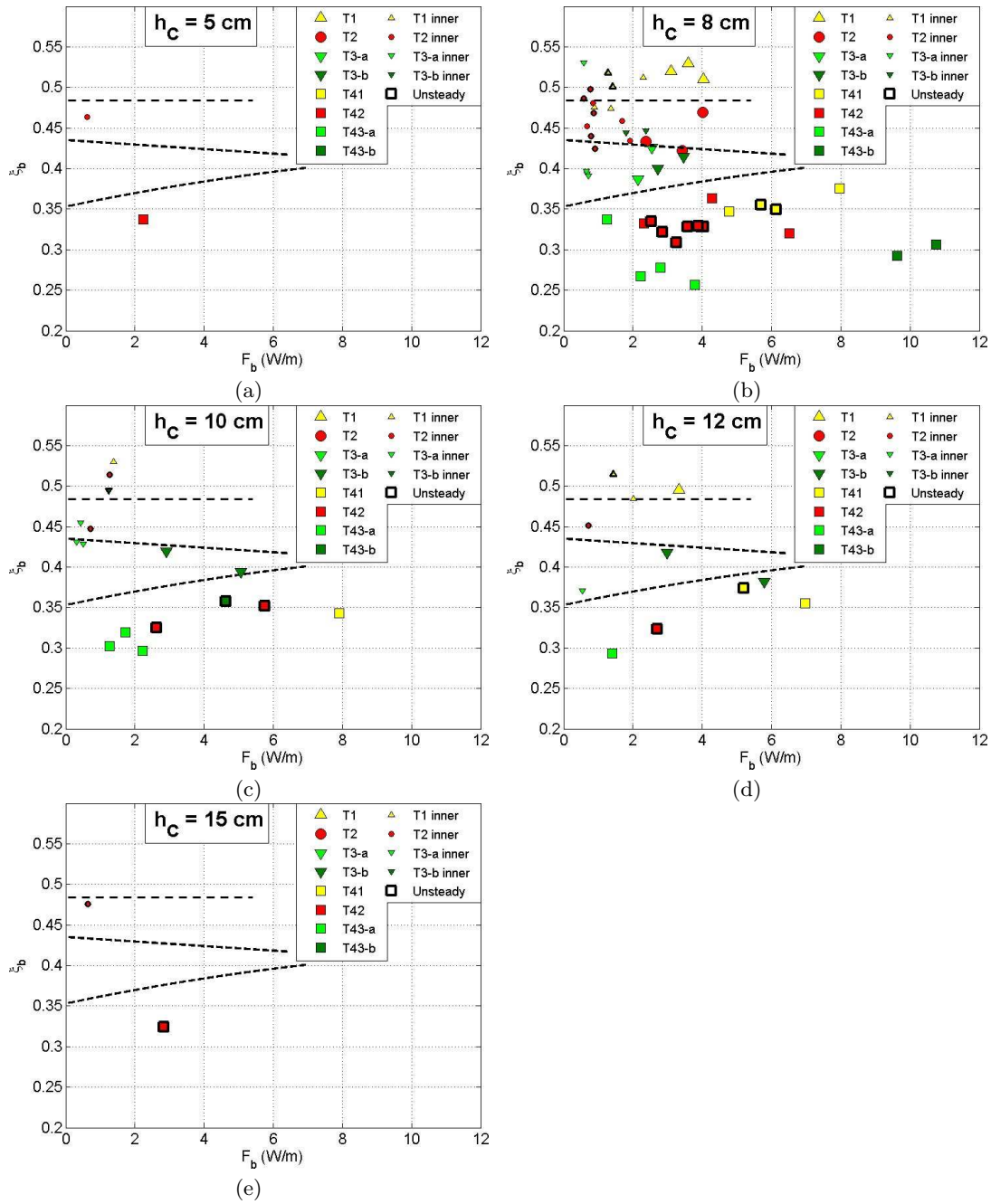


Figure 18. Diagram of bottom typology as a function of wave parameters at the breaker point (F_b, ξ_b) for different cliff height : (a) $h_c = 5$ cm, (b) $h_c = 8$ cm, (c) $h_c = 10$ cm, (d) $h_c = 12$ cm and (e) $h_c = 15$ cm. Representation of symbols are the same as Figure 14.

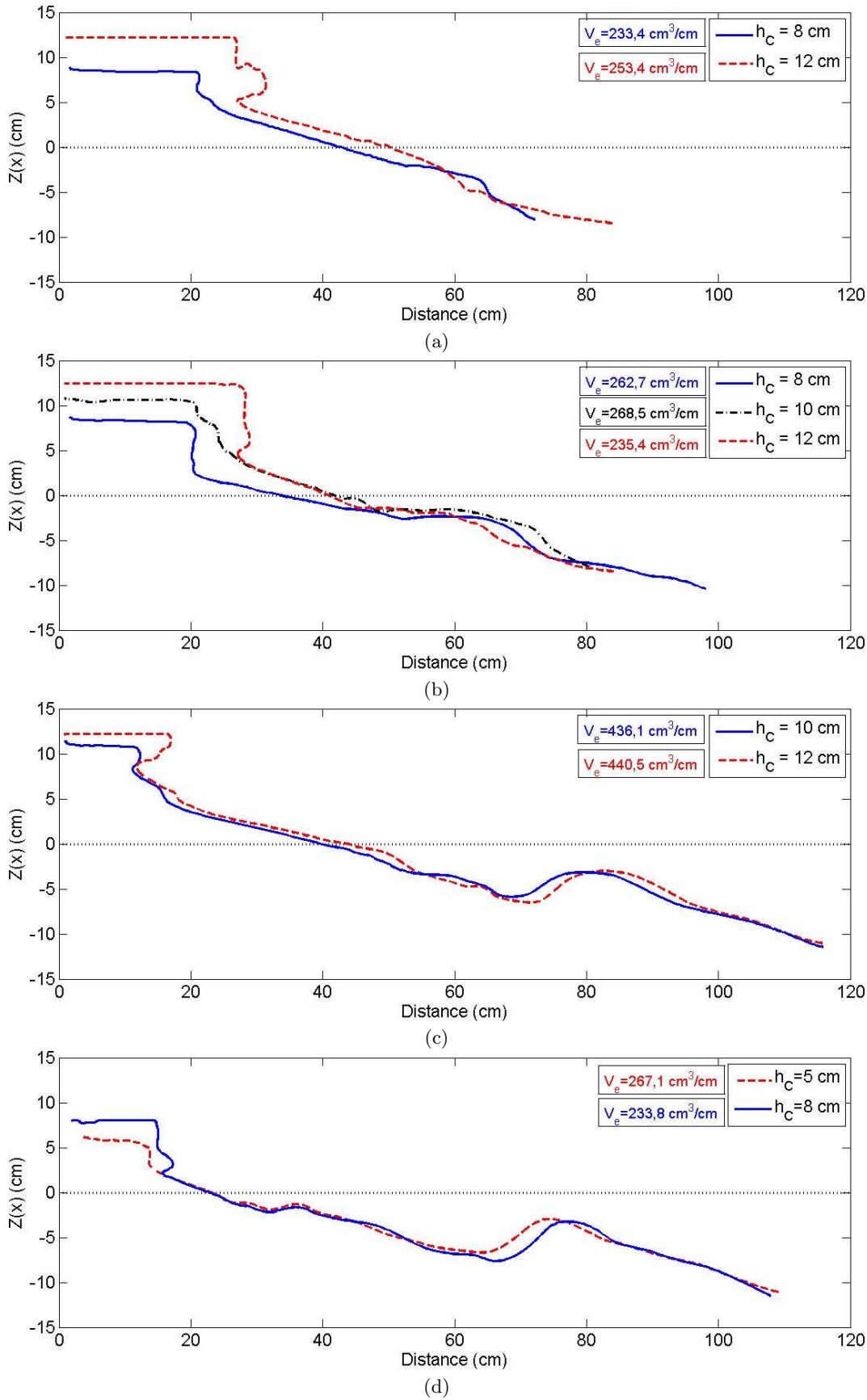


Figure 19. Contours of bottom profiles for different cliff height h_C with similar wave forcing.
 (a) **Type 1** - $h_C = 8\text{cm}$: $(F, \xi) = (1.13 \text{ W/m}, 0.67)$ - $h_C = 12\text{cm}$: $(F, \xi) = (1.09 \text{ W/m}, 0.66)$.
 (b) **Type 3b** - $h_C = 8\text{cm}$: $(F, \xi) = (1.09 \text{ W/m}, 0.50)$ - $h_C = 10\text{cm}$: $(F, \xi) = (1.04 \text{ W/M}, 0.54)$ -
 $h_C = 12\text{cm}$: $(F, \xi) = (1.09 \text{ W/m}, 0.54)$.
 (c) **Type 41** - $h_C = 10\text{cm}$: $(F, \xi) = (2.63 \text{ W/m}, 0.45)$ - $h_C = 12\text{cm}$: $(F, \xi) = (2.39 \text{ W/m}, 0.46)$.
 (d) **Type 42** - $h_C = 5\text{cm}$: $(F, \xi) = (1.12 \text{ W/m}, 0.40)$ - $h_C = 8\text{cm}$: $(F, \xi) = (1.23 \text{ W/m}, 0.39)$.
 V_e is the eroded material.